UCRL-10067

University of California

Ernest O. Lawrence Radiation Laboratory

Berkeley, California

DISCLAIMER

UCRL-10067

UNIVERSITY OF CALIFORNIA

Lawrence Radiation Laboratory
Berkeley, California

Contract No. W-7405-eng-48

ELECTROSTATIC DEFLECTOR CALCULATIONS FOR THE BERKELEY 88-INCH CYCLOTRON

Alper A. Garren, David L. Judd,
Lloyd Smith, and Hans A. Willax

May 4, 1962

ELECTROSTATIC DEFLECTOR CALCULATIONS FOR THE BERKELEY 88-INCH CYCLOTRON

Alper A. Garren, David L. Judd,
Lloyd Smith, and Hans A. Willax

Lawrence Radiation Laboratory
University of California
Berkeley, California

May 4, 1962

ABSTRACT

Early computer calculations showed that an electrostatic channel would have to be very narrow to cause sufficient deflection at high energy. One alternative considered was a system of three electrostatic channels in series, acting as a one-turn regenerative extractor. Such a system could easily achieve the required deflection, but at the expense of simplicity. A magnetic channel to reinforce the electrostatic channel likewise appeared difficult for a variable-energy machine.

Detailed studies of a simple electrostatic channel began with development of an analytic-graphical method of calculating channel efficiency. By this method one can estimate acceptance as a function of radial turn separation, amplitude and frequency of radial oscillations, and channel geometry. A computer code was then developed to compute channel shapes and calculate acceptance more accurately by following the fate of a representative sample of orbits in the presence of the channel. Use of this code indicated that highest acceptance would be obtained if the channel entrance is set out at 39 in. provided the resonances at $\nu_r = 1$ and $\nu_r = 2\nu_z$ could be safely traversed, as was believed possible. Some calculations on transition through the $\nu_r = 2\nu_z$ resonance are presented.

UCRL-10067

ELECTROSTATIC DEFLECTOR CALCULATIONS FOR THE BERKELEY 88-INCH CYCLOTRON †

Alper A. Garren, David L. Judd,
Lloyd Smith, and Hans A. Willax††

Lawrence Radiation Laboratory
University of California
Berkeley, California

May 4, 1962

1. Introduction

This paper presents an account of some of the calculations carried out relative to the beam-extraction system for the Berkeley 88-inch cyclotron. We wished to design a system which could extract at least 10% of the internal beam, for the full range of particles and energies that this machine can accelerate.

The system chosen is a single conventional electrostatic (ES) channel. Various alternatives were considered with varying degrees of thoroughness, as follows:

(i) An ES channel with hot-glass electrodes, to permit higher electric fields. This system had not been proven feasible in a radiation environment.

(ii) Three ES channels in series. This system, discussed in Sec. 2 of this paper, seemed too complex.

(iii) A magnetic channel. This seemed too inflexible for a variable-energy machine, and tests showed it would be difficult to keep the field perturbations small enough on the circulating beam. The beam could not jump a magnetic system without using a regenerative field bump--see (v) below.

---

† Work done under the auspices of the U. S. Atomic Energy Commission.

†† Permanent address: Swiss Federal Institute of Technology, Zurich.

(iv) An ES channel followed by a magnetic channel. Again this seems complex, and possibly not flexible enough.

(v) Regenerative extraction. The use of an azimuthal field bump either to produce beam spill or enhanced turn separation. There did not seem to be time to make sufficient calculations to determine the feasibility of regenerative extraction for our variable-energy machine. Recently Blosser[1]) carried out calculations with our measured field, to see if the efficiency of our existing channel could be enhanced in this way, and we have also made some relevant calculations. As of now this question is still open.

As will be seen, calculations on the single-ES channel gave encouraging results.

We will discuss below some of the computations carried out. The space devoted to the topics treated is not necessarily related to their relative importance, or to the effort devoted to them, but is also determined by novelty and possible theoretical interest.

2. Multiple Electrostatic Deflectors

At an early stage it became apparent that the simple ES deflector (fig. 1) would be strained to provide sufficient deflection for the highest energy (60-MeV) deuterons. This provided an incentive to consider three deflectors, A, B, C arranged in series, as shown in fig. 2, with their electric fields directed outwards, respectively. The first two deflectors, A and B, produce a large radial amplitude in one turn, so that when the beam enters the third deflector it is headed outward enough to be extracted with a moderate field in deflector C.

Qualitative understanding of such a scheme is obtained from the following simplified linear analysis. We suppose that a sequence of deflectors are all arranged parallel to a reference ray traveling through them, that the

electric field is constant in each deflector, and that the magnetic field is uniform. The departure from the magnetic equilibrium orbit x in a deflector is given by†

$$\frac{d^2x}{d\theta^2} + x = \epsilon , \tag{1}$$

where

$$x = \frac{\omega}{c}(R - R_0),$$

$$\omega = \frac{eB_0}{m_0 c},$$

$$\epsilon = \frac{(V/cm)}{300\, B_0\,(G)} .$$

The solution of this equation in the deflector at an angle θ from the beginning of the deflector is

$$\begin{pmatrix} x(\theta) \\ x'(\theta) \end{pmatrix} = \epsilon \begin{pmatrix} 1-\cos\theta \\ \sin\theta \end{pmatrix} + M(\theta/0) \begin{pmatrix} x(0) \\ x'(0) \end{pmatrix}, \tag{2}$$

where

$$M(\theta_2/\theta_1) = \begin{bmatrix} \cos(\theta_2-\theta_1) & \sin(\theta_2-\theta_1) \\ -\sin(\theta_2-\theta_1) & \cos(\theta_2-\theta_1) \end{bmatrix} . \tag{3}$$

If the total deflector angle is λ, then the solution at an angle $\theta - \lambda$ beyond the end of the deflector is

$$\begin{pmatrix} x(\theta) \\ x'(\theta) \end{pmatrix} = M(\theta/\theta-\lambda) \begin{pmatrix} x(\lambda) \\ x'(\lambda) \end{pmatrix} = \epsilon\, M(\theta/\theta-\lambda) \begin{pmatrix} 1-\cos\lambda \\ \sin\lambda \end{pmatrix} + M(\theta/0) \begin{pmatrix} x(0) \\ x'(0) \end{pmatrix}$$

$$= \epsilon \begin{pmatrix} \cos(\theta-\lambda) - \cos\theta \\ -\sin(\theta-\lambda) + \sin\theta \end{pmatrix} + M(\theta/0) \begin{pmatrix} x(0) \\ x'(0) \end{pmatrix} . \tag{4}$$

The first term on the right represents the effect of the deflector and is independent of initial conditions, whereas the second represents the motion in the absence of a deflector. Now imagine a sequence of deflectors and gaps with azimuthal length

---

† For an azimuthally uniform cyclotron a more exact equation is

$x'' + (1-n+n_e)\, x = \epsilon/\gamma$, where $n = \frac{-RdB}{BdR}$, $n_e = -\frac{2\epsilon}{\beta\gamma}$.

λ_i and strength ϵ_i. The ϵ_i may be positive, negative, or zero (for the gaps between deflectors). Then the i^{th} deflector starts at $\theta_{0i} = \sum_{j=1}^{i-1} \lambda_j$ and ends at $\theta_{1i} = \sum_{j=i}^{i} \lambda_j$. From (4) we see that its specific effect at any $\theta \geq \theta_{1i}$ is

$$\begin{pmatrix} x_i(\theta) \\ x_i'(\theta) \end{pmatrix} = \epsilon_i \begin{pmatrix} \cos\left(\theta - \sum_{j=1}^{i} \lambda_j\right) - \cos\left(\theta - \sum_{j=1}^{i-1} \lambda_j\right) \\ -\sin\left(\theta - \sum_{j=1}^{i} \lambda_j\right) + \sin\left(\theta - \sum_{j=1}^{i-1} \lambda_j\right) \end{pmatrix}. \qquad (5)$$

One obtains the solution at the end of a sequence of n deflectors (and gaps) by adding up the effects of all the deflectors, each of which has an effect given by (5), and then adding the original radial oscillation, $x = A \cos(\theta - \phi)$, which goes through unaltered. Thus we obtain (after some rearrangement) the displacement and angle at the end of all the deflectors, at angle $\lambda = \sum_{j=1}^{n} \lambda_j$:

$$\begin{pmatrix} x(\lambda) \\ x'(\lambda) \end{pmatrix} = A \begin{pmatrix} \cos(\lambda-\phi) \\ -\sin(\lambda-\phi) \end{pmatrix} - \epsilon_1 \begin{pmatrix} \cos\lambda \\ -\sin\lambda \end{pmatrix} + \epsilon_n \begin{pmatrix} 1 \\ 0 \end{pmatrix} + \sum_{i=1}^{n-1} (\epsilon_i - \epsilon_{i+1}) \begin{pmatrix} \cos\left(\lambda - \sum_{j=1}^{i} \lambda_j\right) \\ -\sin\left(\lambda - \sum_{j=1}^{i} \lambda_j\right) \end{pmatrix}. \qquad (6)$$

Let us apply this to the three-deflector system of fig. 2. Suppose deflectors A, B, and the gap between have angular lengths λ_1, λ_3, and λ_2, respectively, and that A, B have equal and opposite electric fields, so that $\epsilon_1 = -\epsilon_3 = \epsilon$, $\epsilon_2 = 0$. The system must satisfy the following conditions:

(i) The end of B must not intercept the circulating beam:

$$x(\lambda_1 + \lambda_2 + \lambda_3) > 0.$$

(ii) When the beam has completed one revolution and enters C it must be outside of deflector A: $x(2\pi) > 0$, and as large as possible.

(iii) The beam should be headed outwards, on entering C: $x'(2\pi) > 0$, and as large as possible.

(iv) The deflectors must be outside the dee: $a = \lambda_1 + \lambda_2 + \lambda_3 < \pi$.

What can be concluded from this about the angles λ_1, λ_2, and λ_3? By applying (6) to the above conditions we find, for A = 0:

$$u = \frac{x(a)}{\epsilon} = -\cos a + \cos(a - \lambda_1) + \cos\lambda_3 - 1 > 0, \quad (7)$$

$$v = \frac{x(2\pi)}{\epsilon} = -\cos a + \cos(a - \lambda_3) + \cos\lambda_1 - 1 > 0, \text{ large}, \quad (8)$$

$$w = \frac{x'(2\pi)}{\epsilon} = -\sin a + \sin(a - \lambda_3) + \sin\lambda_1 > 0, \text{ large}, \quad (9)$$

where

$$a = \lambda_1 + \lambda_2 + \lambda_3 < \pi . \quad (10)$$

One way to see the effect of these conditions is to plot curves of $\cos\lambda_1$ vs $\cos\lambda_3$ for fixed a. This is shown in fig. 3 for three values of a. In each case the system point must lie in the triangular region in the upper right. Case (a), a = 120 deg, looks most favorable. Case (c), a = 180 deg, is impossible.

We used these considerations to suggest several arrangements on which more exact computer runs were based. For these runs we used the MURA Ill-Tempered Five Code, with Fourier coefficients chosen to fit the model-magnet measured field. The action of the deflectors was simulated by adding or subtracting a constant term from this magnetic field, according as the electric field is directed inwards or outwards.

These runs qualitatively confirmed the above analytic estimates of the effect of the first two deflectors. Moreover, on entering the third deflector the beam did not appear to have suffered appreciable dispersion. There is considerable dispersion in the third deflector, caused by the fringing field of the magnet, but this affects the single-channel system equally.

TABLE 1

Three-channel deflector system

i	Deflector	Interval λ_i (deg)	Angles covered (deg)	Electric field (kV/cm)
1	A	48	0 - 48	100
2	gap	24	48 - 72	0
3	B	48	72 - 120	-100
4	gap	240	120 - 360	0
5	C	144	0 - 144	100

Table 1 shows one three-channel system studied which should give sufficient deflection to 60-MeV deuterons in our cyclotron. The dispersion is indicated in Table 2 by the effect on two rays displaced from the reference ray.

TABLE 2

Dispersion of three-channel system (of Table 1)

	$\Delta R/R$	Δs	$\frac{\Delta R}{R}$	Δn
Start of A	0.005	0	0	0.00421
Start of C	0.00543	-0.01	-0.00152	0.00525
132° down C	0.00397	.00443	0.0278	0.0424

The clearance of the reference ray from the undeflected equilibrium orbit is 0.9 in. at the end of channel B, and 1.5 in. at the entrance to channel C.

What has been gained by this system is a limitation of the electric fields to 100 kV/cm, as compared with about 160 kV/cm needed for a single channel, with a corresponding increase of channel width by a factor of 2.5 (assuming $V \times E = E^2 d = \text{Const.}$). The price is an enormous increase in mechanical complexity, and filling up space that would otherwise be accessible to probes, etc., so this system was rejected.

3. Analytic Studies of Electrostatic Channel Transmission Efficiency

In this section we present some analytic and graphical methods for estimating the efficiency of electric deflectors. We wished to know how the efficiency depended on particle turn-to-turn separation; on the amplitude and frequency of their radial oscillations; and on channel length, width, and septum thickness.

3.1 JUMPING OVER THE SEPTUM

We were able to develop a purely analytic treatment for the restricted problem of calculating the fraction of the particles that jump a septum of thickness σ, as a function of radial amplitude A, precessional frequency $\delta = \nu_r - 1$, radial turn-to-turn separation of the equilibrium orbits Δr, and σ. This efficiency is calculated subject to the assumptions that the internal beam is of uniform density in equilibrium radius, and random in radial oscillation phase, in the vicinity of the deflector.

A septum, of width σ, is located between r_s and $r_s + \sigma$ at $\theta = 0$. We consider a particle of amplitude A at some particular phase $\underline{\Phi}$ of radial oscillation. Suppose we start counting turns at equilibrium radius $r_0 = r_s - A$. This guarantees that the particle has not previously reached the septum. Actually we cannot specify r_0 this closely--it might vary from $r_s - A$ by an amount Δr, the equilibrium radius gain per turn, so the orbit, on the first turn we look at it, is given by

$$r_0(\theta) = r_s - A + \lambda \Delta r + A\cos(\nu_r \theta - \phi), \quad 0 \leq \lambda \leq 1, \quad 0 \leq \underline{\Phi} \leq 2\pi. \tag{11}$$

After n turns this same orbit will have a radius at the septum azimuth of $r_n = r_n(0)$:

$$r_n = r_s + (n \pm \lambda)\Delta r - A\left[1 - \cos(2\pi n\delta - \underline{\Phi})\right], \quad \delta = \nu_r - 1 . \tag{12}$$

All particles in the internal beam are characterized by their values of λ, $\bar{\Phi}$ within the given ranges; our uniformity assumptions imply a uniform density in λ, $\bar{\Phi}$ space. To calculate the efficiency F for jumping the septum we have to calculate what fraction of the λ, $\bar{\Phi}$ rectangle (of area 2π) belongs to particles missing the septum. To do this we rewrite (12) as follows:

$$y_n \equiv \frac{r_n - r_s}{A} = n\frac{\Delta r}{A} + \lambda \frac{\Delta r}{A} - [1 - \cos(2\pi n\delta - \bar{\Phi})] \times = \lambda \frac{\Delta r}{A} \qquad (13)$$

and ask what fraction of the, λ, $\bar{\Phi}$ rectangle (of area $\frac{2\pi\Delta r}{A}$) corresponds to particles missing the septum. The conditions for missing or hitting the septum on the N^{th} turn are:

$$y_n < 0, \quad n < N,$$

and

$$y_N > \sigma/A \text{ , jump septum,}$$
$$0 \leq y_N \leq \sigma/A \text{ , strike septum.} \qquad (14)$$

It is useful to represent these conditions graphically. This is done in fig. 4 for A = 0.25 in., σ = 0.05 in., Δr = 0.1 in., $2\pi\delta$ = 30 deg. Hence $\sigma/A = 0.2$, $\Delta r/A = 0.4$. To understand the graph the above conditions are written explicitly, using (13), as follows

$$z + n\frac{\Delta r}{A} < [1 - \cos(2\pi\delta - \bar{\Phi})] , \quad n < N,$$

and

$$[1 - \cos(2\pi N\delta - \bar{\Phi})] \leq z + N\frac{\Delta r}{A} \leq \frac{\sigma}{A} + [1 - \cos(2\pi N\delta - \bar{\Phi})], \text{ hit septum,} \qquad (15)$$

$$z + N\frac{\Delta r}{A} > \frac{\sigma}{A} + [1 - \cos(2\pi N\delta - \bar{\Phi})], \text{ jump septum.}$$

In fig. 4 the abscissa is $\bar{\Phi}_n = \bar{\Phi} - 2\pi n\delta$, the ordinate is $z_n \equiv n\frac{\Delta r}{A} + \lambda\frac{\Delta r}{A}$. On turn n = 0 all our particles are in the rectangle ADFE. On each successive turn each point $(\bar{\Phi}_n, z_n)$ is displaced by $(-2\pi\delta, \Delta r/A) = \vec{\Delta}$, so rectangle n = 0

moves up to rectangle n = 1, etc. Curves α and β are defined by

$$\alpha: \ (\bar{\Phi}_n, z_n) = (\bar{\Phi}_n, 1-\cos\bar{\Phi}_n) ,$$
$$\beta: \ (\bar{\Phi}_n, z_n) = (\bar{\Phi}_n, \frac{\sigma}{A} + (1 - \cos\bar{\Phi}_n)) , \qquad (16)$$

whereas α_- and α_+ represent the locus of points on α one turn previously and one turn later, respectively (i.e., $\alpha_+ = \alpha + \vec{\Delta}$, $\alpha_- = \alpha - \vec{\Delta}$). Since the conditions (15) are equivalent to

$$z_n < \alpha, \quad n < N ,$$
$$\alpha \leq z_N \leq \beta, \quad \text{hit septum},$$
$$z_N > \beta, \quad \text{jump septum},$$

particles between curves α and β hit the septum, and those above β jump the septum provided on the previous turn they were below α. Thus on turn n = 0 that part of the rectangle above β represents particles jumping the septum, that part below α represents particles that make another turn, after which they occupy part of the n = 1 rectangle--and again the same three things can happen.

The analysis is simplified by taking the original area to be the dark-shaded zone between α and α_+, rather than the rectangular zone n = 0. This is legitimate because both zones have the same area, and every beam particle must pass through each zone. The new zone is A' B' B'' A'' + C' D' D'' C''. The division into two subzones occurs because of the first condition. Point C' is the intersection of curves α and α_-. Had we followed curve α any further to the left beyond C', then on the previous turn the points on α would have been points on α_- above α, contrary to the first condition.

In this way we have chosen a representative zone such that on the previous turn all the particles are in the light-shaded area below α--and thus have not yet reached the septum--while on the turn in question all the representative particles

are in the process either of hitting or jumping over the septum.

To calculate the acceptance efficiency we have to take the ratio of the dark-shaded area above β to the total dark-shaded area, which is the same as the original rectangle area ($= 2\pi \frac{\Delta r}{A}$) :

$$F = \frac{\text{Area } (a_+ - \beta)}{\text{Area } (a_+ - a)} = \frac{\text{Area } (a_+ - \beta)}{2\pi \Delta r/A} \tag{17}$$

This calculation of F can easily be done by plotting a graph like fig. 4, and using a planimeter to obtain the phase areas needed. If the precession angle $2\pi\delta \ll 1$, the calculation of F can also be done analytically as follows. From fig. 5 it is clear that the fraction of particles that hit the septum is

$$\bar{F} = 1 - F = \frac{1}{2\pi} \int_0^{2\pi} d\bar{\Phi} \cdot \bar{f} = \frac{\overline{AB}}{\overline{AC}} = \frac{x_\sigma}{\Delta} \ . \tag{18}$$

To obtain $\bar{f}$ we write

$$\frac{z_A}{\bar{\Phi} - \bar{\Phi}_A} = \frac{1 - \cos\bar{\Phi}_A}{\bar{\Phi} - \bar{\Phi}_A} = \frac{\Delta r}{2\pi\delta A} \equiv \eta \equiv \tan\psi, \tag{19a}$$

$$\frac{z_B}{\bar{\Phi} - \bar{\Phi}_B} = \frac{1 - \cos\bar{\Phi}_B + s}{\bar{\Phi} - \bar{\Phi}_B} = \eta, \quad s = \sigma/A, \tag{19b}$$

hence

$$\Delta z = z_B - z_A = \eta(\bar{\Phi}_A - \bar{\Phi}_B) = \eta \Delta\bar{\Phi} \ , \tag{20a}$$

$$\cos\bar{\Phi}_A - \cos\bar{\Phi}_B = \eta(\bar{\Phi}_A - \bar{\Phi}_B) - s = \eta \Delta\bar{\Phi} - s. \tag{20b}$$

If the precession angle $2\pi\delta$ and /or σ are small enough, $\Delta\bar{\Phi}$ will be small enough to justify replacing $\cos\bar{\Phi}_A - \cos\bar{\Phi}_B$ by $-\Delta\bar{\Phi} \sin\bar{\Phi}_A$, so that from (20) we obtain

$$\Delta\bar{\Phi} \approx \frac{s}{\eta + \sin\bar{\Phi}_A} \ , \tag{21}$$

and

$$x_\sigma = \sqrt{\Delta z^2 + \Delta\underline{\Phi}^2} = \sqrt{\eta^2+1}\cdot\frac{s}{\eta+\sin\underline{\phi}_A},$$

$$\Delta = \sqrt{(2\pi\delta^2) + (\frac{\Delta r}{A})^2} = 2\pi\delta\sqrt{\eta^2+1},$$

whence

$$\overline{r} = x_\sigma/\Delta = \frac{s}{2\pi\delta}\frac{1}{\eta+\sin\underline{\phi}_A}. \tag{22}$$

From eq. (19a) we have

$$\underline{\Phi} = \underline{\Phi}_A + \frac{1-\cos\underline{\Phi}_A}{\eta}. \tag{23}$$

This can be used to replace $\underline{\Phi}$ by $\underline{\Phi}_A$ as the integration variable in (18)--however one must exclude those values of $\underline{\Phi}_A$ given by smaller values of $\underline{\Phi}_A$, otherwise the same $\underline{\Phi}$ values would be counted twice. The excluded region in $\underline{\Phi}_A$, if any, runs from $\underline{\Phi}_{A1}$ to $\underline{\Phi}_{A2}$, where $\underline{\Phi}_{A1}$ is at the maximum of $\underline{\Phi}$ with respect to $\underline{\Phi}_A$, and $\underline{\Phi}_{A2}$ is a larger value of $\underline{\Phi}_A$ for which $\underline{\Phi}(\underline{\Phi}_{A2}) = \underline{\Phi}(\underline{\Phi}_{A1})$. From (23), this means

$$\underline{\Phi}_{A1} = \pi + \sin^{-1}\eta, \tag{24}$$

$$\underline{\Phi}_{A2} - \frac{\cos\underline{\Phi}_{A2}}{\eta} = \pi + \sin^{-1}\eta + \frac{\sqrt{1-\eta^2}}{\eta}, \quad \underline{\Phi}_{A2} > \underline{\Phi}_{A1}. \tag{24}$$

The excluded zone occurs if, and only if, $\eta < 1$. From (23) we have $d\underline{\Phi} = \left(1 + \frac{1}{\eta}\sin\underline{\Phi}_A\right) d\underline{\Phi}_A$, so from (18) and (24) we get

$$\overline{F} = \frac{\sigma}{\Delta r}, \quad \eta > 1,$$

$$\overline{F} = \frac{\sigma}{\Delta r}\left[2\pi + \underline{\Phi}_{A1} - \underline{\Phi}_{A2}\right], \quad \eta < 1. \tag{25}$$

These formulas should be treated with some caution because of the approximation (21). The graphical method should be used if more accuracy is desired. It is not surprising that $\overline{F} = \sigma/\Delta r$ wherever $\eta > 1$, $\frac{\sigma}{\eta-1} \ll 1$ or

$$F = 1 - \frac{\sigma}{\Delta r} \qquad (26)$$

wherever

$$2\pi(\nu_r - 1) \ll \frac{\Delta r}{\sigma + A}.$$

3.2 CHANNEL ACCEPTANCE

The graphical method explained above for the septum can now be extended to the whole channel. However, since rather sweeping assumptions are made about the path of the orbits in the channel, we only claim qualitative validity for the results.

Consider the equilibrium orbit that just grazes the septum, as shown in fig. 6, with radius $r_e(\theta)$. We start counting turns for a particle with amplitude A, phase ϕ, where the crest of its oscillation just touches the septum or is within Δr of doing so. Its displacement from the equilibrium orbit, so long as it is outside the deflector, is x_n^0, where

$$x_n^0(\theta) = r_n(\theta) - r_e(\theta) = (n + \lambda)\,\Delta r - A\,[1 - \cos(2\pi n\delta + \nu_r\theta - \Phi)],$$

$$0 \leq \Phi < 2\pi, \quad 0 \leq \lambda < 1. \qquad (27)$$

We assume the channel is shaped for an equilibrium orbit. If the electric field in the channel is constant then the deflected equilibrium orbit (called the reference ray) departs from the undeflected equilibrium orbit roughly quadratically in θ. Hence, the inside edge of the septum, of radius $r_b(\theta)$, is given by $r_b = r_e + x_b$, where $x_b(\theta) = (\frac{\theta}{\lambda})^2 h$. (28)

Here λ is the azimuthal length of the channel and h is the radial displacement of its end point. We assume that all particles in the channel follow the same path as they would outside, except that we add the deflection term $(\frac{\theta}{\lambda})^2 h$. This assumption is relatively good near the entrance, and gets worse as the channel goes through the cyclotron fringe-field. With this assumption, the displacement of our particle in the channel from the reference equilibrium

orbit is x_n^i, where

$$x_n^i(\theta) = x_n^0(\theta) + x_b(\theta). \tag{29}$$

The surfaces of interest are the following, given in terms of their displacement from $r_e(\theta)$ (we will sometimes refer to large/small r surfaces as top and bottom, respectively);

end of septum E_:	$\theta = 0,\ 0 \leq x \leq \sigma$	
bottom of septum B_:	$x_b(\theta) = (\frac{\theta}{\lambda})^2 h$	
top of septum T_:	$x_t(\theta) = x_b(\theta) + \sigma$	(30)

The various things that might happen to a particle on the n^{th} turn are:

(a) strike bottom of septum (B_) at θ	$x_n^0(\theta) = x_b(\theta)$
(a') pass under channel	$x_n^0(\theta) < x_b(\theta)$
(b) strike end of septum (E_)	$0 \leq x_n^0(\theta) \leq \sigma$
(b') enter channel	$x_n^0(\theta) > \sigma$
(c) strike top of septum (T_) at θ	$x_n^i(\theta) = x_t(\theta)$
(c') pass over top of septum	$x_n^i(\theta) > x_t(\theta),\ 0 \leq \theta \leq \lambda$
(d) strike bottom of electrode at θ	$x_n^i(\theta) = x_1(\theta)$
(d') pass under electrode	$x_n^i(\theta) < x_1(\theta),\ 0 < \theta < \lambda$
(e) strike end or top of electrode	$x_n^i(\theta) \geq x_2(\theta)$.

Transmission on the n^{th} turn requires (a)' for $n < N$, and (b)', (c'), and (d') for turn N. Written explicitly, the above conditions, using eqs. (27)-(30), are as follows:

(a) : (a)'	$(n+\lambda)\frac{\Delta r}{A} \leq (\frac{\theta}{\lambda})^2 \frac{h}{A} + [1 - \cos(\phi - 2\pi n\delta + \nu_r\theta)]$,	any $\theta \leq \lambda$ hit T_ $0 < \lambda < \theta$ under T_
(b) : (b)'	$[1 - \cos(\phi - 2\pi n\delta)] \leq (n+\lambda)\frac{\Delta r}{A} \leq \frac{\sigma}{A} + [1 - \cos(\phi - 2\pi n\delta)]$,	hit T_ enter channel

(c) : $(n+\lambda)\frac{\Delta r}{A} \geq \frac{\sigma}{A} + [1-\cos(\underline{\phi}-2\pi m\delta - \nu_x\theta)]$, any $\theta \leq \lambda$ hit T_

(c)' $0 \leq \lambda \leq \theta$ over T_

(d) : $(n+\lambda)\frac{\Delta r}{A} \leq \frac{\sigma+d}{A} + [1-\cos(\underline{\phi}-2\pi m\delta - \nu_x\theta)]$, any $\theta \leq \lambda$ hit B+

(d)' $0 \leq \lambda \leq \theta$ under B+

(e) : $(n+\lambda)\frac{\Delta r}{A} > \frac{\sigma+d}{A} + [1-\cos(\underline{\phi}-2\pi m\delta)]$, hit E+ or T+.

As in the case of septum jumping alone, these conditions may be graphed (fig. 6). Again we want to know what fraction of the λ, $\underline{\phi}$ rectangle corresponds to transmission on some turn n. We plot in $[\underline{\phi}-2\pi m\delta,\ (n+\lambda)\frac{\Delta r}{A}]$ space the curves bounding the inequalities (a)', (c)', and (d)'. These curves are labeled as follows: α = lower envelope of curves (a), $\beta_1 = (n+\lambda)\frac{\Delta r}{A} = (1-\cos(\underline{\phi}-2\pi m\delta))$, $\beta_2 = \beta_1 + \sigma/A$, γ = upper envelope of curves (c), δ = lower envelope of curves (d), $\epsilon = \beta_2 + (d/A)$.

Again the n = 0 rectangle is the normalizing area, and we replace it by the equivalent zone between curves α and $\alpha+$, where $\alpha+$ is curve α shifted by $\Delta = (-2\pi\delta,\ \Delta r/A)$ as before. This area is broken into subzones as follows:

hit B_ : over α, under β_1

hit E_ : over β_1, under β_2

hit T_ : over β_2, under γ

C(through channel) : over γ, under δ

hit B+: over γ, under δ

T_ or B+: under γ, over δ (see which curve comes from smallest θ)

E or T+: over ϵ

The procedure is to graph all the above curves and color the areas def and above. The fraction that suffer the various fates described above is obtained by measuring each sub-area, and dividing by the normalizing area $2\pi\Delta r/A$. As before, the total zone $\alpha+-\alpha$ might break up into two subzones, broken at the

intersection of a_+ and a_-.

Figure 6 illustrates the critical effect precession can have. There are three possible (triangular) zones corresponding to transmission (C). As δ becomes positive, curve a_+ moves into the left hand zone. As δ goes to zero a_+ moves to the right until nothing remains in the left-hand triangle, but some comes in from the upper triangle (this is usually much less). Finally, for large negative δ ($\nu_r < 1$), one can exploit the right-hand triangle.

The latter possibility, $\nu_r < 1$, occurs at larger radii as one approaches the maximum of $rB(r)$. Since $p \propto rB(r)$, the turn separation Δr is larger there, so curve a_+ is higher than for $\nu_r > 1$, which also enhances transmission. Consequently, δ should either be as positive as possible, or sufficiently negative to get into the right-hand triangle.

A comparison of figs. 6a, b, c, shows the effect of amplitude A on transmission for fixed δ, and the results are combined in fig. 6d. Figure 7 shows a case with negative δ.

3.3 EFFECT OF SPIRAL HILLS

The turn separation Δr at the beginning of the deflector should be maximized in order to enhance jumping of the septum, and this determines the best width for the channel entrance.

If the magnetic field at the septum radius r_0 is written

$$B(r,\theta) = B(r_0)\{1 + \mu' x + \sum_n [a_{3n}\cos(3n\theta) + b_{3n}\sin(3n\theta)] + \ldots\},$$
$$x = (r - r_0)/r_0, \qquad (31)$$

then the equilibrium orbits are given approximately[5] (for a three-sector machine) by

$$r_e(\theta) = \frac{1}{8}[a_3\cos(3\theta) + b_3\sin(3\theta)] = \frac{1}{8}A_3\cos[3(\theta - \theta_H)], \qquad (32)$$

where θ_H is approximately at the center of a hill and $A_3 = \sqrt{a_3^2 + b_3^2} = \sqrt{2}F$,

F = flutter.

The radial gain per turn then is

$$\Delta r(\theta) = \frac{dr_c(\theta)}{dn} = \frac{dr_0}{dn}\left\{1 + \frac{\sqrt{2}}{g} F\left[\cos 3(\theta-\theta_H) + 3 \tan \zeta \sin 3(\theta-\theta_H)\right]\right\}. \quad (34)$$

where

$\tan \zeta = r_0 \frac{d\theta_H}{dr}$ is the spiral angle. For a machine with appreciable spiral, the maximum Δr is near

$$3(\theta-\theta_H) = \pm \pi/2, \text{ for } \zeta \gtrless 0, \text{ or } \theta \approx \theta_H \pm 30 \text{ deg}. \quad (35)$$

Thus, if the hills are about 60 deg wide, we see that the channel should start at the end or beginning of a hill, depending on whether the spiral is with or against the particle rotation, respectively.

Of course the choice of initial angle will also affect the amount of radial deflection attainable with a given electric field. For low-enough energy machines the beam might be deflected sharply enough to have most of the deflector in a valley. Then, perhaps one should have the spiraling with the particle rotation and start deflection at the beginning of a valley, so both turn separation and deflection will be optimized. For higher energies the channel runs through both hill and valley, and the deflection is less sensitive to position of the deflector, especially if the spiral is against the particle rotation.

It is not completely obvious that spiral in the particle-rotation direction is best, for while it means deflection can start in a valley, the orbit is headed inward there. Also, the hill field falls off faster with radius. For our cyclotron the spiral is counter to the particle rotation, a choice not entirely governed by deflector considerations.

4. Channel Efficiency Computer Studies

4.1 DEFLECTION CODE CYBOUT

To facilitate more precise predictions of channel efficiency a specialized computer code for the IBM 704 was designed by one of the authors, and written by Owens[2] at Oak Ridge National Laboratory. This code, called CYBOUT, is intended both to calculate channel wall coordinates and transmission efficiencies.

The heart of the CYBOUT code is the Oak Ridge general orbit code GOC, which integrates orbits in a magnetic field specified on a polar-coordinate grid in the median plane. It simulates the effect of an electric channel by an appropriate change in the original magnetic field, which is valid if the channel is shaped to the orbits, so that the electric field is always perpendicular to them. The effect of a magnetic "channel" is specified as a field modification, given as a function of perpendicular distance from the iron septum. First-harmonic perturbations of the field for regenerative extractions can be introduced by specifying the amplitude and phase of the first harmonic as functions of radius.

For an electric channel one gives the electric field in the form

$$E(\theta) = E_0 + E_1(\theta-\theta_0) + E_2(\theta-\theta_0)^2, \qquad (36)$$

where θ_0 is the beginning angle of the channel. A reference ray is chosen by specifying initial conditions p, r_i, p_{ri} at some $\theta_i \leq \theta_0$. The code integrates this reference orbit into and through the channel (from θ_0 to θ_1), and beyond to θ_f. From the r, p_r of this orbit, $E(\theta)$, the channel voltage V_e, the septum thickness σ, and the relative distances between the reference orbit and the two walls, the channel wall coordinates are calculated and stored.

To estimate acceptance efficiency, one specifies initial conditions for a representative set of orbits at radii sufficiently smaller than that of the channel to be

sure they have not yet hit it. Each orbit is then integrated with acceleration; and the computer keeps track of whether each orbit stays outside the channel, strikes some part of the septum, or enters the channel. If the particle enters the channel, its orbit is integrated with the E-modified magnetic field. The integration stops when the orbit hits the septum or electrode, or goes through the channel (to θ_f). By recording, with CYBOUT, the fates of a sufficiently large and representative set of particles, one may estimate the efficiency of the channel.

The addition to, or replacement of, the electric field in the channel by a magnetic field from an iron septum simply alters the effective field in the channel, and adds a magnetic perturbation to the field below the channel. Addition of a first-harmonic bump modifies the field everywhere. The code can also simulate the effect of several channels in series.

4.2 NUMERICAL CALCULATIONS

Most of our numerical calculations with the CYBOUT code were concerned with the design of a single ES channel for 60-MeV deuterons, since this case requires the largest electric field. It will be recalled from the graphical analysis that channel acceptance appears possible either for small positive precession $\delta = \nu_r - 1$, or a considerably larger negative value. The latter corresponds to ES extraction from conventional cyclotrons, and a major objective of our analysis was to determine the feasibility of extraction with positive precession. This we considered a safer way to extract, since we feared it might prove impossible to bring the beam through the $\nu_r = 1$ and $\nu_r = 2\nu_z$ resonances in the fringe-field which would occur before δ was sufficiently negative to provide good channel efficiency. Consequently, we began our studies with the code putting the channel at 37 in. where $\nu_r \approx 1.03$.

The first task was to determine values of E_0, E_1, E_2 [eq. (36)] that give an external beam 5 to 10 in. away from and parallel to the yoke.

This is done by trial-and-error variation of the E_i, and plotting of the external orbits. Then one sets the electrode voltage V_e at a value given by the empirical sparking limit:

$$V_e E = K = \text{constant} \qquad (37)$$

This constant is about 10^4 kV^2/cm for copper, and perhaps twice that for hot glass. Since the channel is always narrowest at the start, this limit controls E_0 only. (It is important to deflect as much as possible at the beginning, since this is most effective in terms of maximizing displacement at the channel exit.)

After we had proper values of the E_i, acceptance studies were run. These involved shooting representative particles at the deflector, as described above. We ran five different energies, spanning ΔE, the energy gain per turn; and at each of those energies we ran particles whose initial r, p_r were located on a rectangular grid about the equilibrium orbit for the energy involved. These grids generally included radial amplitudes of 1/16, 1/8, and 1/4 in.

For these 37-in. studies the relevant parameters were typically $\nu_r = 1.03$, $\Delta r = 0.04$ in. (for 70-kV dee voltage), $\sigma = 0.03$ in., $\lambda = 108$ deg, $E_0 \approx 185$ kV/cm, $V_0 = (10^4/185)$ kV. We found the results were quite sensitive to various parameters at our disposal. Thus toward the end of the channel the beam is dispersed most strongly by the fringe-field. Consequently one gains a good deal by flaring the channel at the downstream end to conform to the beam envelope. It also turned out that acceptance was enhanced by letting the reference ray be headed inward from the equilibrium orbit corresponding to 1/16 in. radial amplitude; i.e., it was best to tilt the channel inwards relative to an equilibrium orbit. It was also advantageous to run the reference ray much closer to the inside of the channel than to the outside. We found that with the parameters noted above we were able to obtain extraction efficiencies of 10 to 15% for amplitudes up to 1/8 in.

This acceptance is perhaps satisfactory, but not outstanding. Meanwhile we had been urged by Richardson[3]) to try larger radii, since his experience with the Berkeley electron model had convinced him that particles would even spill out without difficulty. If the beam could negotiate the resonances, channel efficiency should improve at larger radii because the turn separation increases near the peak of rB(r), the precession becomes strongly negative, and less E-field is required to deflect, allowing the channel to be wider. Therefore we decided to try CYBOUT acceptance runs further out, and check the resonances later.

The CYBOUT code was used with the channel entrance at 38, 38.5, and 39 in. For 38 in. we obtained essentially zero acceptance--as expected from the graphical analysis, because δ was negative but small. However at 38-1/2 and 39 in., especially 39 in., we obtained very encouraging results. At 39 in. the turn separation Δr had increased to about 0.06 in., $\nu_r \approx 0.8$, and E ≈ 65 MeV. We took a reference ray 1/16 in. outside and headed inward by 1/16 in./r radians relative to the corresponding equilibrium orbit, and used a flared channel shape: E = (160-359^2)kV/cm, (this shape fits the 1/8 in. amplitude orbits fairly well). With this configuration we were able to obtain about 50% transmission efficiency for particles with A ≤ 1/8 in., and about 20% for A ≈ 1/4 in. This regime of extraction corresponds to the graphical analysis of fig. 7. The energy spread of the transmitted particles is 0.3 to 0.4 MeV. These particles leave the channel as if they originated at a point source 34 in. upstream from the channel exit, with an angular spread of 1/2 deg. The point source moves inward with energy, about 0.1 in./MeV. The moderate effect of the fringe-fields in the channel on the axial motion is shown on three sample orbits in fig. 8.

There are possible hazards to extraction at 39 in. One is that the beam will be lost vertically at 38.5 in., where $\nu_r = 2\nu_z$ from the coupling

resonance there. Another is that the radial beam quality will deteriorate in passing through the $\nu_r = 1$ radial instability. For reasons that will be discussed in the next section, neither of these effects looked too bad, so we shaped the channel for extraction at 39 in. However, we are not committed to this since considerable flexibility has been built into the channel. It is 108 deg long and jointed at 72 deg, and each of the six relevant points, two at each end and two at the joint, have about 3 in. of radial motion.

The proper shaping of the channel field and choice of reference ray was accomplished, needless to say, after considerable experimentation with CYBOUT, plotting of deflected orbits, etc.

Unfortunately, the optimal channel shape for high-energy deuterons is not optimal for particles in lower fields. We felt the problem would be less severe then because the channel would need a weaker field, and so could be wider. We found that the 50-MeV protons, at about 12 kG, would fit in the channel. Since at lower fields there is more flutter, the orbits wiggle more, so the upstream septum curvature should be greater, and we may need to put another joint on the septum.

The statistics of our acceptance run with the 39-in. channel are shown in figs. 9 and 10, the first showing the energy spread in units of one turn (or 140 kV), and the second the fraction of particles vs amplitude that go through the channel, hit the septum, etc.

5. Bringing the Beam to a Channel Beyond the $\nu_r = 1$ Radius

5.1 RADIAL STABILITY

It is not certain that the beam can be accelerated out to a radius where ν_r is sufficiently less than one to exploit the right-hand acceptance triangle (fig. 6a) and still retain sufficiently good radial and axial beam quality. In our cyclotron at least, there is no problem so far as phase lag is concerned—this is about 30 deg at 39 in., where $\nu_r \approx 0.8$. So far as radial loss of beam quality is concerned, acceleration runs on the GOC (general orbit code) showed that the beam suffers hardly any distortion on passing through $\nu_r = 1$ for $A \leq 1/8$ in., and only moderate distortion up to 1/4 in (see fig. 11).

However, if there is a small first-harmonic component in the field, a large radial oscillation will be introduced. This effect may be estimated as follows. The radial equation of motion may be written approximately

$$\frac{d^2x}{d\theta^2} + \nu_r^2 x = \frac{B_1}{B_2} \cos\theta, \tag{38}$$

where

$$x = (r - r_e) r_0 .$$

if we set

$$h = \frac{B_1}{B_0} \frac{1}{\nu_r^2} , \quad \psi = \nu_r \theta = (1 + \delta)\theta ,$$

then

$$\frac{d^2x}{d\psi^2} + x = h \cos(1 - \delta)\psi. \tag{39}$$

Since ν_r is decreasing, we linearize near $\nu_r = 1$ and set $\delta = -\epsilon\theta$. Integration of the resulting equation involves a Fresnel integral. Most of the change in x occurs over a comparatively small range in θ, so one gets approximately the correct shift by integrating between $\pm\infty$. The result is that traversal of the $\nu_r = 1$ radius with a first-harmonic component B gives

a radial amplitude

$$A = R \frac{B_1}{B_0} \sqrt{\frac{\pi}{\epsilon}} \quad . \tag{40}$$

The quantity $\epsilon = d\nu_r/d\theta$ can be obtained, for example, by running the equilibrium orbit code at equal small increments of energy. For 60-MeV deuterons in our cyclotron, with 70-kV dee voltage, we have R = 37 in., $B_0 = 17 \times 10^3$ G, whence $A \approx 1/7\ B_1$ in. This estimate was well-confirmed by the orbit code.

There are two bad consequences of such a radial amplitude. The first is that if the ES channel has been shaped to fit equilibrium orbits, it will not accept large amplitudes. Thus our calculations showed acceptance dropping from 50% to 20% between 1/8 in. and 1/4 in. amplitude, and is about zero at 3/8 in. Secondly, the radial amplitude can feed into the vertical oscillations $\nu_z = \nu_r/2$. This occurs at about 38.5 in. in our cyclotron, before the optimal radius for channel acceptance.

5.2 AXIAL STABILITY

The coupling (Walkinshaw) resonance at $\nu_r = 2\nu_z$ is a formidable barrier, and it is usually regarded as impassable. However, it appears that with care, safe passage through this resonance can be obtained, if the fringe-field is suitably shaped. This is possible because both the strength of the driving force at the resonance and the resonance width depend critically on the radial derivatives of the average magnetic field and on the amplitude of radial oscillation.

In our cyclotron, the Walkinshaw resonance is never traversed in the isochronous region of the magnetic field, but only in the fringe-field, where the large negative gradient of the average field causes ν_z to become large. In this region the strongest nonlinear terms in both radial and axial motion arise from the average field only.

It is first of all instructive to consider the situation if there are no flutter-dependent terms, as in ordinary cyclotrons. We save only the largest nonlinear terms in the fringe-field region and find that the equations for $x = (r - r_0)/r_0$, $y = z/r_0$ are approximately

$$\frac{d^2x}{d\theta^2} + \nu_x^2 x = \frac{\mu''}{2} y^2 + \frac{\mu'''}{2} xy^2 - \frac{\mu'''}{6} x^3 ,$$

$$\frac{d^2y}{d\theta^2} + \nu_y^2 y = \mu'' xy + \frac{\mu'''}{2} x^2 y - \frac{\mu'''}{6} y^3 , \qquad (41)$$

where $\mu^{(n)} = (r_0/B(r_0))\,(d^n B(r_0)/dr_0)$. These equations follow from a Hamiltonian

$$H = \left(\frac{P_x^2}{2} + \frac{P_y^2}{2}\right) + \left[\frac{\nu_x^2}{2} x^2 + \frac{\nu_y^2}{2} y^2 - \frac{\mu''}{2} xy^2 + \frac{\mu''}{24} (x^4 - 6x^2y^2 + y^4)\right] . \qquad (42)$$

If one examines the potential term, one finds a set of equipotentials about the origin, representing stable motion, and then a set going to infinity. The outermost stable equipotential crosses the x and y axes at

$$x_{max} = \frac{1}{\sqrt{8}} \frac{\nu_r}{2} \sqrt{\frac{6}{-\mu'''}} , \quad y_{max} = \nu_z \sqrt{\frac{6}{-\mu'''}} . \qquad (43)$$

In our machine $\nu_r = 2\nu_z$ near $R = 38$ in., where $\mu''' \approx -100$, so $z_{max} \approx 4$ in. Thus the motion will never become truly unstable before the particles hit the dee, at $z \approx 3/4$ in. At $\nu_r = 2\nu_z$ we have, from (43), that $x_{max}/y_{max} = 1/\sqrt{8}$. For much smaller amplitudes the equipotentials cross the x and y axes with intercepts in ratio of 1/2. Now since we can tolerate only $z < 3/4$ in., we must keep $A_r < 1/4$ in. to be safe, if the particles stay long enough in the stop band to move an appreciable distance around the equipotential. But we have seen that to keep $A_r < 1/4$ in. requires the first-harmonic amplitude $B_1 < 2$ G when $\nu_r \approx 1$. Consequently, safe passage of the coupling resonance

is assured for our cyclotron conditions if the beam is centered, has radial oscillations under 1/4 in., and if $B_1 < 2$ G at 37 in.

The situation would have been worse had y_{max}, eq. (43), been smaller. Indeed, unless one keeps $z_{max} = R\, y_{max} < g/2$, where g is the dee gap, the beam will be lost axially even without any coupling resonance.

On the other hand, the above requirements on A_r and B_1, might be relaxed. The fact that z_{max} is so large for our cyclotron means that we can really ignore the last term in eq. (42), so the motion is linear in y. The term $\frac{\mu'''}{2}\, x^2 y$ may be replaced by $\frac{\mu'''}{2}\, x^2\, y$ (ν_z^2 already contains a term $-\frac{\mu'''}{2}\,\frac{F^2}{(N^2-1)^2} = \frac{-\mu'''}{2}\, x_{eq}^2$ see ref. 5) Appendix 2). Hence we write, for the effective vertical frequency,

$$\nu_y^2 = \nu_{y0}^2 - \frac{\mu'''}{4}\, A_x^2, \tag{44}$$

where ν_{y0}^2 is the axial frequency for zero radial amplitude (ref. 5), Appendix 2), and $A_x = A_r/r$.

Having justified the neglect of nonlinear terms in y, we now generalize the axial equation to include the most important flutter-dependent terms. It is well known that the effect of the axial motion on the radial is practically negligible, hence the radial motion is taken as given.‡ It is now convenient to follow a method derived by Veksler and Hagendoorn[3] for putting the axial equation in a form derivable from the Hamiltonian K:†

$$K(Y, P_y, \theta) = \frac{1}{2}\, P_y^2 + \frac{1}{2}\,\Omega^2(\theta) Y^2, \tag{45}$$

where

$$Y = f^{1/2}\, y, \quad p_y = f^{-1/2}\left(P_y + \frac{1}{2} f^{-1}\, \dot{f}\, Y\right), \tag{46}$$

$$\Omega^2(\theta) = f\, h - \frac{1}{4}(f^{-1}\dot{f})^2 + \frac{1}{2}\,\frac{d}{d\theta}\,(f^{-1}\dot{f}),$$

---

†We use a dot for $d/d\theta$ and a prime for $r_0\,\frac{d}{dr} = \frac{d}{dx}$.

‡However, the above considerations, predicting $y < 3\,A_x$ whenever $x < x_{max}$ remain valid, so whenever the succeeding analysis predicts violations of this rule, it may be disregarded.

and

$$f = (1 + x)\sqrt{1 - p_x^2}, \quad h = p_x \sqrt{1 - p_x^2}\, \dot{M} - (1 + x)M'. \tag{47}$$

Here we suppose the magnetic field is given in the median plane by

$$B(r, \theta) = B(r_0)[1 + M(r, \theta)]. \tag{48}$$

If one uses equilibrium-orbit values for x and p_x in the above equations, (45) becomes a Hill equation from which the axial frequency ν_y may be obtained. It can also be obtained by using the smooth approximation, as two of the authors have done[5]. However, the Hamiltonian method is most convenient for seeing the effect of the radial betatron oscillations. We write the radial motion in terms of the equilibrium orbit and free oscillation as

$$x(\theta) = x_e(\theta) + u(\theta). \tag{49}$$

If M is expanded as in ref. 5) then

$$M(x, \theta) = \mu' x + \mu'' \frac{x^2}{2} + \cdots + \Sigma + x\Sigma' + \cdots$$

$$Q^2(x, \theta) = -\left[\mu' + \left(\frac{\Sigma}{2} + \Sigma' - \frac{\Sigma^2}{2}\right) + \left(1 + \frac{5}{2}\mu' + \mu''\right)x \right. \tag{50}$$

$$+ \left(-\frac{1}{2}\Sigma + \frac{5}{2}\Sigma' + \Sigma''\right)x + \left(-\frac{1}{2}\frac{1}{2}\mu' + \frac{9}{4}\mu'' + \frac{1}{2}\mu'''\right)x^2$$

$$\left. + \dot{\Sigma} p_x - \frac{1}{2} p_x^2 \right]$$

where

$$\Sigma = \sum_{n=1}^{\infty} C_n \cos n(\theta - \Theta_n),$$

we find (see eq. (45) and Appendix 3 of ref. 5)) that the radial oscillation is given approximately by ($A_x = A_r/r_0$, and we set $\Theta_N = 0$)

$$u = A_x \cos(\nu_x \theta - \bar{\Phi}) + \frac{A_x C_N \tan \zeta}{N^2 - 4}\left[\sin N\theta \cos(\nu_x \theta - \bar{\Phi}) \right.$$

$$\left. - \frac{2\nu_x}{N} \cos N\theta \sin(\nu_x \theta - \bar{\Phi})\right], \tag{51}$$

where $\zeta = \Theta_N'$ is the spiral angle. The largest terms in Q^2 involving u are $-\mu'' u - \frac{5}{2}\Sigma' u$. Picking out the parts that have frequency ν_x gives

$$\delta Q^2 = b \cos(\nu_x \theta - \bar{\Phi}), \quad b = -\left[\mu'' + \frac{5}{4} \frac{C_N \cdot N \tan \zeta}{N^2 - 4} \right] A_x . \tag{52}$$

Hence the Hamiltonian may be written $K = K_0 + K_1$, where K_0 is the Hamiltonian with $u = 0$ and K_1 is the perturbation due to the free radial oscillation u:

$$K_1 = \frac{1}{2} Y^2 b \cos \nu_x \theta , \tag{53}$$

where we have dropped the radial phase angle $\bar{\Phi}$.

When $K_1 = 0$ the Y motion is given, to sufficient accuracy, by

$$Y = A \cos (\nu_y \theta - \psi). \tag{54}$$

We use the method of variation of constants, regarding A and ψ as slowly varying parameters. Thus

$$K_1 = \frac{1}{2} A(\theta) \cos [\nu_y \theta - \psi (\theta)]^2 \cdot b \cos \nu_x \theta . \tag{55}$$

If a canonical transformation is made from Y, P_y to $\frac{\nu_y}{2} A^2$, ψ—the new Hamiltonian, as pointed out in ref. [4])—is just K_1, eq. (55); and from it the equations of motion for A, ψ can be derived using

$$\frac{d}{d\theta}\left(\frac{\nu_y}{2} A^2 \right) = \frac{\partial K_1}{\partial \psi} , \quad \frac{d\psi}{d\theta} = - \frac{\partial K_1}{\partial (\frac{\nu_y}{2} A^2)} . \tag{56}$$

If we keep only the terms of frequency $\nu_- = 2\nu_y - \nu_x$, the result is approximately

$$\frac{dA}{d\theta} = - \frac{bA}{4\nu_y} \sin 2\chi , \quad \chi = \psi - \frac{\nu_-}{2} \theta , \tag{57a}$$

$$\frac{d\chi}{d\theta} = - \frac{b}{4\nu_y} \cos(2\chi) - \frac{1}{2} \nu_- + \frac{b^2}{16 \nu_y \nu_+} , \quad \nu_\pm = 2\nu_y \pm \nu_x , \tag{57b}$$

which has the integral invariant (ignoring the b^2 term)

$$C = - \frac{\nu_-}{2} A^2 + \frac{b}{4\nu_y} A^2 \cos 2\chi . \tag{58}$$

It is easy to see from (58) that instability occurs ($A \to \infty$) when

$$\left| \frac{2\nu_- - \nu_y}{b} \right| < 1, \text{ unstable axial motion.} \tag{59}$$

The situation is complicated by the fact that $\nu_\pm$ are not constant as the particle is being accelerated through the stop-band. Let us approximate them by

$$\nu_\pm = \dot{\nu}_\pm \theta, \qquad \chi = \psi - \frac{\dot{\nu}_- \theta^2}{2} . \tag{60}$$

so that the equations (57) becomes

$$\frac{1}{A} \frac{dA}{d\theta} = - \frac{b}{4\nu_y} \sin 2\chi - \frac{\pi^2 \dot{\nu}_+ b^2}{24 \nu_y^2 \nu_+^4} \tag{61}$$

$$\frac{d\chi}{d\theta} = - \frac{b}{4\nu_y} \cos (2\chi) - \dot{\nu}_- \theta + \frac{b^2}{16 \nu_y \nu_+}$$

Two limiting cases can be considered. In one the transiton through the stop-band is fast compared to the time required to lock into phase $\chi = -\pi/4$, in the other the reverse is true. To see which domain applies, and the amount of amplitude growth in each case, we compare those various times.

The lock-in time θ_ℓ is obtained by solving (57) for χ when $\nu_- = 0$. One finds

$$|\tan (\tfrac{\pi}{4} + \chi)| = |\tan (\tfrac{\pi}{4} + \chi_0)| \exp (- \frac{b}{2\nu_y} \theta) \tag{62}$$

so that a reasonable lock-in time to take would be when the exponent is 2, or

$$\Delta\theta_\ell = \frac{4\nu_y}{b} . \tag{63}$$

To get the stop-band width $\Delta\theta_s$ we replace ν_- by $\dot{\nu}_- \Delta\theta$ in (59) (written as an equality):

$$\Delta\theta_s = \frac{b}{\nu_y \dot{\nu}_-} , \tag{64}$$

so that the condition for locking into the phase $\chi = -\pi/4$ during most of the transition through the resonance is $\Delta\theta_s >> \Delta\theta_\ell$, or

$$b >> b_\ell = \nu_x \sqrt{\dot{\nu}_-} \quad , \quad \text{lock-in} \quad . \tag{65}$$

If this is the case, $b >> b_\ell$, then we approximate the total amplitude growth by integrating the A equation with $\sin 2\chi \simeq \sin 2\chi_\ell = [1 - (2\nu_y \dot{\nu}_-/b)^2 \theta^2]^{\frac{1}{2}}$ between $\theta = \pm \Delta\theta_s/2$. The result is $A_f/A_i = \exp[-b^2/(16 \nu_y^2 \dot{\nu}_-)]$. Had we used the maximum growth rate across the whole stop-band we would have the same formula with a 4 replacing the 16. Short of a rigorous integration of the motion,† a compromise on the value 8 seems reasonable:

$$A_f/A_i \approx \exp[\pi b^2/(8 \nu_y^2 \dot{\nu}_-)] \quad , \quad \begin{matrix}\text{slow transition} \\ b >> \nu_x \dot{\nu}_-^{1/2}\end{matrix} \quad . \tag{66}$$

On the other hand, when $b << b_\ell$, χ will not change much during transition through the stop-band. Since in (61) the $\dot{\nu}_- \theta$ term is generally the largest, we solve χ by successive approximations to obtain

$$\chi(\theta) \approx \chi_0 - \frac{\dot{\nu}_- \theta^2}{2} - \frac{b}{4\nu_y}\sqrt{\frac{\pi}{2\dot{\nu}_-}}\left[\cos(2\chi_0) C(\dot{\nu}_- \theta^2) + \sin(2\chi_0) S(\dot{\nu}_- \theta^2)\right] , \tag{67}$$

where C and S are the Fresnel integrals, $C(z) = \int_0^{\sqrt{2z/\pi}} \cos\frac{\pi}{2} u^2 \, du$, etc. We ignore the C, S terms and substitute in the A equation, whence

$$\ln \frac{A(\theta)}{A_0} = -\frac{b}{4\nu_y}\sqrt{\frac{\pi}{2\dot{\nu}_-}}\left[\sin 2\chi_0 \, C(\dot{\nu}_- \theta^2) - \cos 2\chi_0 \, S(\dot{\nu}_- \theta^2)\right] , \tag{68}$$

$$\frac{A_f}{A_i} \simeq \exp\left[-\frac{b}{4\nu_y}\sqrt{\frac{\pi}{\dot{\nu}_-}} \sin(2\chi_0 - \tfrac{\pi}{4})\right] , \quad \begin{matrix}\text{fast transition} \\ b << \nu_x \dot{\nu}_-^{1/2}\end{matrix} \tag{69}$$

Here χ_0 is the (random) axial phase at the center of the stop-band.

---

†We intend to make a more exact integration of eqs. (57a) and (61), for all parameter values—if necessary by computer.)

For the fringe field of our cyclotron $b > b_\ell$ when $A_r \approx 1/4$ in., so that eq. (66) is the relevant one to apply.

In order to see the explicit dependence on field-shape parameters we evaluate $\dot{\nu}_-$ using (44) and the expressions in the Appendices of ref. [5]) for ν_r^2 and ν_z^2, keeping only the largest terms [the $\mu^{(n)}$ increase roughly as r^n in the fringe-field region]:

$$\dot{\nu}_- \approx \frac{d}{d\theta}(2\nu_y - \nu_x) \approx \frac{1}{\nu_y}\,\frac{5}{4}\left\{\dot{\mu}' + \dot{\mu}'''\left[\frac{C_N^2}{4(N^2-1)^2} + A_x^2\right]\right\} \tag{70}$$

but

$$\frac{d}{d\theta} = \frac{dx}{dr}\left(\frac{dr}{d\gamma}\,\frac{d\gamma}{dn}\right)\frac{dn}{d\theta}\,\frac{d}{dx} = \frac{\epsilon_0 \cos\phi_{rf}}{2\pi\beta^2\gamma^3(1+\mu')}\,\frac{d}{dx}\,,$$

$$\epsilon_0 = \frac{\Delta E}{m_0c^2}\,, \quad \gamma = \frac{E}{m_0c^2}\,,$$

where ϕ_{rf} is the rf phase angle of the particle. Hence for slow transition, $b > b_\ell$, we have from (52), (66), and (70)

$$\frac{A_f}{A_i} \approx \exp\left(\frac{\pi^2\beta^2\gamma^3\left(\mu'' + \frac{5}{4}\,C_N\,\frac{N\tan\zeta}{N^2-4}\right)^2(1+\mu')\,A_x^2}{-5\epsilon_0\cos\phi_{rf}\,\nu_y\left\{\mu'' + \left[\frac{C_N^2}{4(N^2-1)^2} + A_x^2\right]\mu^{iv}\right\}}\right)\,. \tag{71}$$

For 60-MeV α particles in our cyclotron, the resonance occurs at 38.3 in., where $\mu'' \approx 6$, $C_N \approx 0.25$, $\zeta \approx 55^\circ$, $\Delta E = 140$ kV, $N = 3$, $\beta = 0.183$, $\nu_y \approx 0.5$. For moderate (< 1 in.) radial amplitudes the μ'' terms dominate and (71) may be written

$$\frac{A_f}{A_i} \approx \exp\frac{2\beta^2\gamma^3\mu''A_x^2}{\nu_y\epsilon_0\cos\phi_{rf}}\,. \tag{72}$$

and for the numbers quoted above, this gives $A_f/A_i \approx \exp(20\, A_r^2)$ for A_r in inches, or a factor of 3.5 for $A_r = 1/4$ in. If the original axial amplitude is over 1/4 in., then particles will be lost to the dees. To avoid this A_r must be kept less than 1/4 in., so again B_1 should be under 2.5 G.

When the radial amplitude A_x gets very large eq. (71) reduces to

$$\frac{A_f}{A_i} \approx \exp\left[\frac{2\beta^2\gamma^3(\mu'' + \frac{5}{4} C_N \frac{N \tan \zeta}{N^2 - 1})^2}{-\nu_y \epsilon_0 \mu^{iv} \cos \phi_{rf}}\right] \qquad (73)$$

If μ'' dominates the flutter term, then we may compare the exponents for small and large A_r (we use subscripts S and L to refer to resonance with small and large A_r, respectively):

$$\frac{(\ell n\, A_f/A_i)_S}{(\ell n\, A_f/A_i)_L} = \frac{\mu''_S\, A_{xS}^2\, \mu_L^{iv}}{(\mu''_L)^2} = \frac{\mu''_S}{(\mu''_L)^2} \frac{d\mu''_L}{dr} \frac{(A_{rS})^2}{r}. \qquad (74)$$

For our cyclotron this ratio is about unity for $A_{rS} = 1/4$ in. if $\frac{\mu''_S}{\mu''_L} \approx 5$, which is quite plausible, since the large radial amplitude A_{rL} increases ν_y [c.f. eq. (44)], causing the resonance to occur at a smaller radius, where μ'' is smaller. Moreover, a large radial amplitude can cause the beam to spill out of the cyclotron radially before the coupling resonance is reached. Thus we reach the paradoxical conclusion that to survive axially, the radial amplitude must either be kept quite small or very large. Our cyclotron abhors moderation.

Certain observations have been made tending to confirm the above analysis. Firstly, orbits have been integrated through the resonance with acceleration, using the Oak Ridge General Orbit Code[6] with the measured 88-inch cyclotron field. We set the initial axial amplitude at 1/4 in. and took radial amplitudes of 0, 1/8, 1/4, and 1/2 in. The factors of increase are shown in table 3.

TABLE 3

Increase of axial amplitude after acceleration through $\nu_x = 2\nu_y$ resonance vs radial amplitude, from computer runs and from theory

n	A_r(in.)	(A_f/A_i) computer	(A_f/A_i) slow, eq. (66)	$\frac{A_f}{A_i}$ fast, eq. (69)
0		1.0	1.0	1.0
1/8			1.37	0.7 to 1.5
1/4		0.4 , 2.7	3.5	0.5 to 2
1/2		224, 143	150	0.2 to 5

These runs are in qualitative agreement with the theory above, and show that the transition from fast to slow traversal occurs at about A_r = 1/4 in. †

Secondly, there is experimental confirmation. When the beam was centered at 39 in. (beyond the resonance) shadow probe measurements showed radial amplitudes up to 1/8 in. and of half the intensity that the beam had at 30 in. (before the resonance), where shadow-measurements showed up to 1/4 in. amplitude. The interpretation is that when A_r > 1/8 in. the resonance caused axial blowup. Similar evidence from the UCLA cyclotron has been adduced by Richardson[7]. Furthermore, Richardson, by introducing about 20-G first harmonic in the 88 inch cyclotron, induced radial beam spill without serious axial blowup, which is in agreement with the above arguments about large radial amplitudes.

---

† Both these theoretical results and the computer runs ignore the y^2, p_y^2 terms in the radial equations, which take energy out of the radial oscillations when y gets large; so the driving term $b \approx \mu'' A_r$ in the axial equation decreases, limiting the total y-growth. A more complete treatment of the problem, which we hope to carry out probably would reveal at the momentum vector for the combined radial and axial oscillations moves on some equipotential surface in a 3-dimensional space, corresponding to those in eq (44), which is ellipsoidal for small amplitudes. We have been discussing only the equatorial motion.

A. Direct First-Harmonic Effects

If there is any first harmonic in the field, trouble can ensue at $\nu_y = 1/2$. First of all, the field bump itself contributes to $Q^2(\theta)$, eq. (50), an amount $-\Sigma'_1 = -[C'_1 \cos(\theta-\Theta) + C_1 \tan\zeta_1 \sin(\theta-\Theta_1)]$, where C_1, Θ_1, and ζ_1 are the amplitude, azimuth, and spiral angle of the first harmonic. Secondly, there will be a contribution $-\mu'' x_1$, where x_1 is the first-harmonic part of the equilibrium orbit [see ref. 5) eq. (11)]:

$$x_1 = -\frac{C_1}{\mu'} \cos(\theta - \Theta_1) \qquad (75)$$

so the perturbation in the Hamiltonian is (setting $\Theta_1 = 0$):

$$K_2 = \frac{1}{2} Y^2 \left[\left(\frac{\mu'' C_1}{\mu'} - C'_1 \right) \cos\theta - C_1 \tan\zeta_1 \sin\theta \right] \qquad (76)$$

By comparing (76) with (53) it is clear that we can use all of the above theory of the coupling resonance, if we replace b in eq. (52) by

$$b_1 = \left[\left(\frac{C_1 \mu''}{\mu'} - C'_1 \right)^2 + C_1^2 \tan^2 \zeta_1 \right]^{1/2}, \qquad (77)$$

and ν_x by 1. The dominant term here is $C_1 \mu''/\mu'$, so whenever A_x occurs it should be replaced by C_1/μ'. Since we have $\mu' \approx 0.1$ where $\nu_y = 1/2$, we find that $C_1 = B_1/B_0 = 1/1600$ ... corresponds to $A_x = 1/4$ in. But in a 12-kG field this would be 7 G, which gives rise to $A_x \approx 1$ in. Hence we see that this resonance is far less important, in our cyclotron, than the coupling resonance.

B. Use of First Harmonic to Aid Extraction

Some orbit computer runs have been carried out corresponding to the situation in which beam spill was induced by Richardson (sec. 5) He ran the outer valley correcting coils so that they produced a first-harmonic amplitude rising slowly from 30 in. to a peak of about 20 G at 37 in., with the peak of the bump 220 deg counter-clockwise from the south (beam-leaving) dee gap. The computed orbits developed radial amplitudes of about 3 in. at about 37 in., and then spilled(one third of them into the dee, however). The divergence of the spill-beam was very large. However, a few turns before the spill, and near the deflector-entrance azimuth, the orbits were very concentrated in r, p_r space; showed complete turn-to-turn separation (for an initial 1/8-in. -amplitude distribution); and jumped sufficiently to enter the channel with almost 100% efficiency. Unfortunately, the orbits also have about 10% less energy than they would without a field bump. This could mean that another 100-kV/cm electric field might be required to deflect--but this might be mitigated by the larger radial momentum of the bumped orbits. Further investigation of this possibility is planned.

Acknowledgments

Many persons have contributed to the theoretical work on the deflection system for our cyclotron. Extensive computations have been carried out by H. G. Blosser at Michigan State on the possibility of regenerative extraction with the existing field-shapes, deflector channel, and dee voltage. Of especial interest are the radial phase plots he compiled, with various bump-strengths and without a bump. It is not appropriate for us to describe this work -- we hope he does -- but we certainly wish to thank him for enlarging our understanding of our cyclotron.

The most important work of writing and operating the relevant computer codes was carried out by H. C. Owens, partly at Oak Ridge National Laboratory. He programmed the codes CYBOUT and GOC, and carried out many of the relevant machine computations. Indespensible aid with computations has also been rendered by A. S. Kenney, J. D. Young, and D. N. Brainard.

We have profited from close collaboration with our opposite numbers at ORNL. In particular the design of the deflection code CYBOUT, was much aided by discussions with R. S. Bender and R. H. Bassel. We wish to thank F. T. Cole and Elisabeth Chapman at MURA for their help with the Ill Tempered Five Code.

It goes without saying that E. L. Kelly has played a decisive role in this work. We are very grateful to J. R. Richardson for many fruitful discussions and cogent advice. We also wish to thank A. S. Sessler for discussions of the resonances and R. Peters for discussions on the mechanics of the system.

REFERENCES

[1] H. G. Blosser (Michigan State University) private communication.

[2] H. C. Owens, Three Computer Programs for Calculating Cyclotron Orbits, Lawrence Radiation Laboratory Report UCRL-10083, April 1962, Nucl. Instr. and Meth. (to be published).

[3] J. R. Richardson (University of California at Los Angeles) private communication.

[4] N. F. Verster and H. L. Hagedoorn, Orbits in an AVF Cyclotron, Philips Research Laboratory Report 3623 (1960).

[5] Lloyd Smith and A. A. Garren, Orbit Dynamics in the Spiral-Ridged Cyclotron, Lawrence Radiation Laboratory Report UCRL-8598, Jan. 1959 (unpublished).

[6] H. C. Owens and T. A. Welton, An IBM 704 Code for Studying Particle Orbits in Cyclotron Fields, Oak Ridge National Laboratories Report CF 59-11-3, Nov. 1959 (unpublished).

[7] J. R. Richardson, paper presented at the International Conference on Sector-Focused Cyclotrons, Los Angeles, April 1962, Nucl. Instr. and Meth. (to be published).

FIGURE CAPTIONS

Fig. 1. Schematic diagram of single electrostatic deflector for the Berkeley 88-inch cyclotron.

Fig. 2. Schematic diagram of triple ES deflector system.

Fig. 3. Graphical construction for three-deflector system [see eqs (7)-(10)]. λ_1 = length of channel A (deg), λ_2 = gap A-B, λ_3 = length of B, $\alpha = \lambda_1 + \lambda_2 + \lambda_3$. Each plot shows λ_3 vs λ_1, for fixed α. Conditions (7)-(10) require that point (λ_1, λ_3) be away from hatched side of each curve, and restrict point to be in triangular region at upper right. (Fig. 3a: $\alpha = 120^\circ$, fig. 3b: $\alpha = 150^\circ$, fig. 3c: $\alpha = 180^\circ$.)

Fig. 4. Graph representing efficiency for jumping a septum of width σ, by particles with turn separation Δr, amplitude A, precession frequency $\delta = \nu_r - 1$. This graph represents $2\pi\delta = 30^\circ$, $\sigma/A = 0.2$, $\Delta r/A = 0.4$. (see Text).

Fig. 5. Diagram to indicate derivation of approximate formula for septum-jumping efficiency.

Fig. 6a. Graphical construction for ES channel efficiency. Shaded areas are proportional to the fraction of particles striking various parts of the deflector or passing through, according to letter key in schematic diagram at upper right. Normalizing area (all shaded area) = $360 \cdot \Delta r/A$ degrees. Unshaded lettered areas are potentially available, by changing $\Delta r/A$ or δ.

Fig. 6b. Channel acceptance for 1/16-in. radial amplitude. Other parameters are the same as for fig. 6a.

Fig. 6c. Channel acceptance for 1/4-in. radial amplitude. Other parameters are the same as for fig. 6a.

Fig. 6d. Channel transmission efficiency vs amplitude from graphs 6a, b, c.

Fig. 7. A channel acceptance diagram for $\nu_r < 1$.

Fig. 8. Axial motion in deflector channel.

Fig. 9. Energy and amplitude distribution of particles transmitted by channel at 39 in. from computer runs. Integration of all orbits was begun about 1/2 in. inside of channel, with energy spread corresponding to one turn (140 kV). Turn number is number of turns orbits made before entering channel. Shadings represent different radial amplitudes.

Fig. 10. Percentage of particles transmitted by channel or striking various parts of structure, as functions of radial amplitude.

Fig. 11a. Radial distortion of particles accelerated through $\nu_r = 1$ (at 37.5 in.); amplitude/of grid = $\frac{1}{8}$ in.

Fig. 11b. Radial distortion of particles accelerated through $\nu_r = 1$ (at 37.5 in.); amplitude/of grid = $\frac{1}{4}$ in.

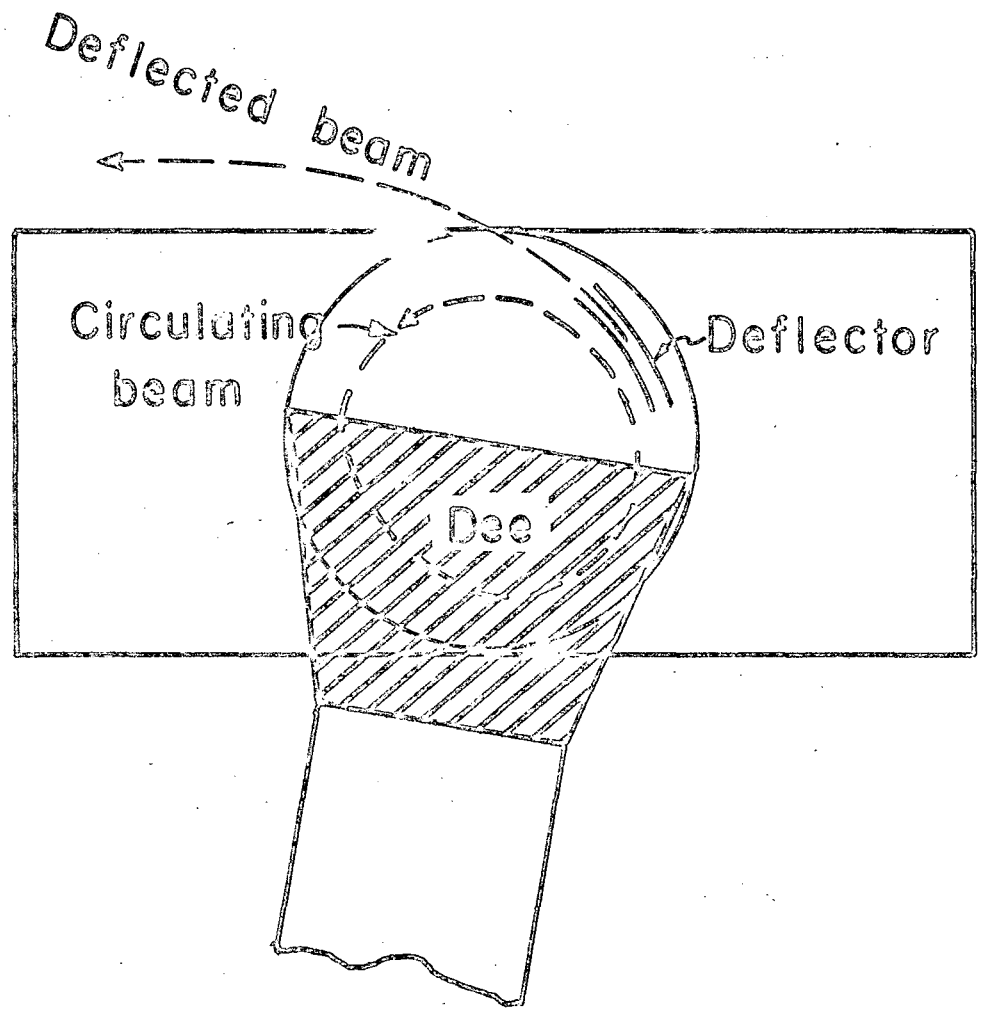

MU-26364
UCRL-10067
Fig. 1

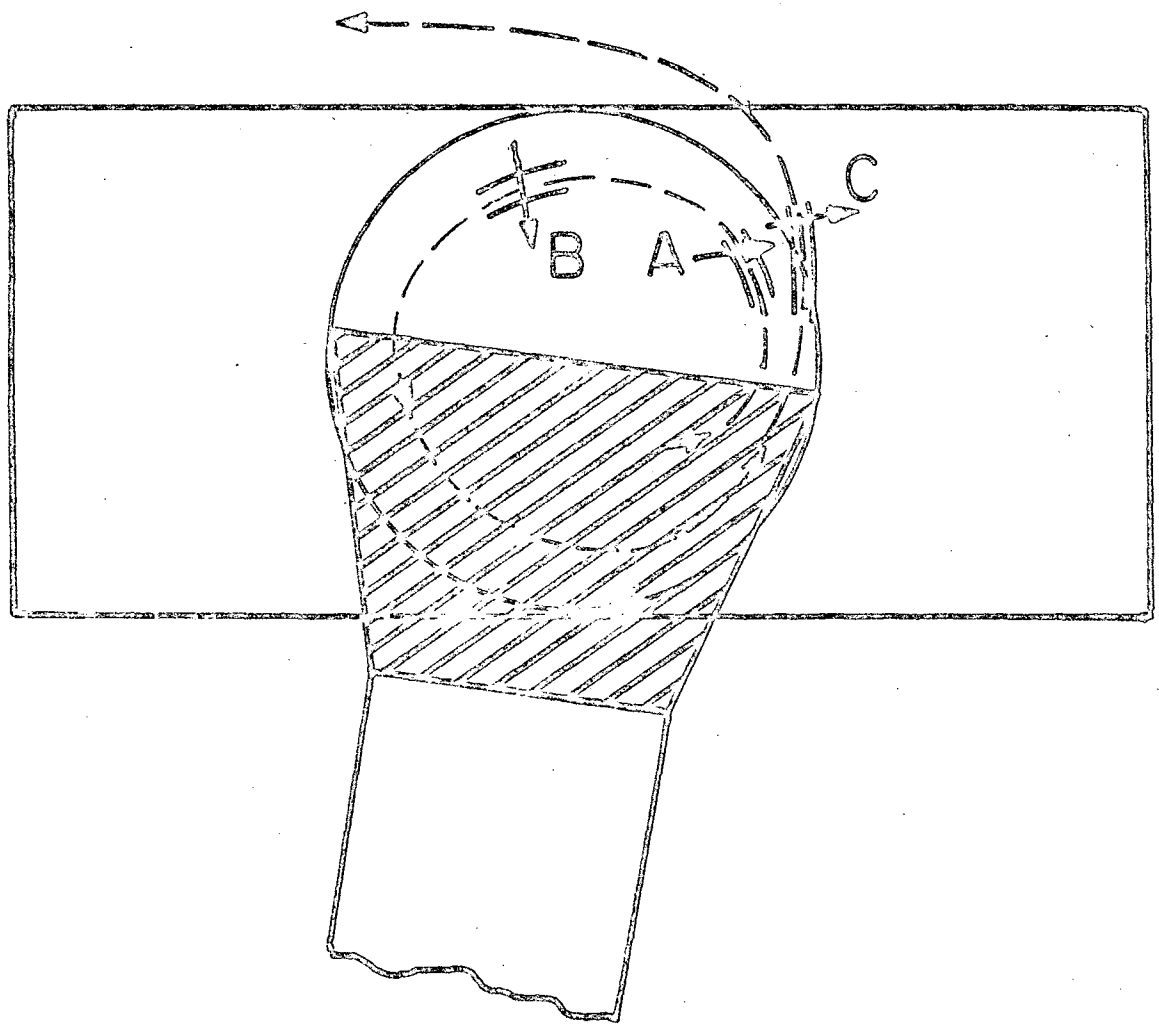

MU-26363
UCRL-10067
Fig. 2

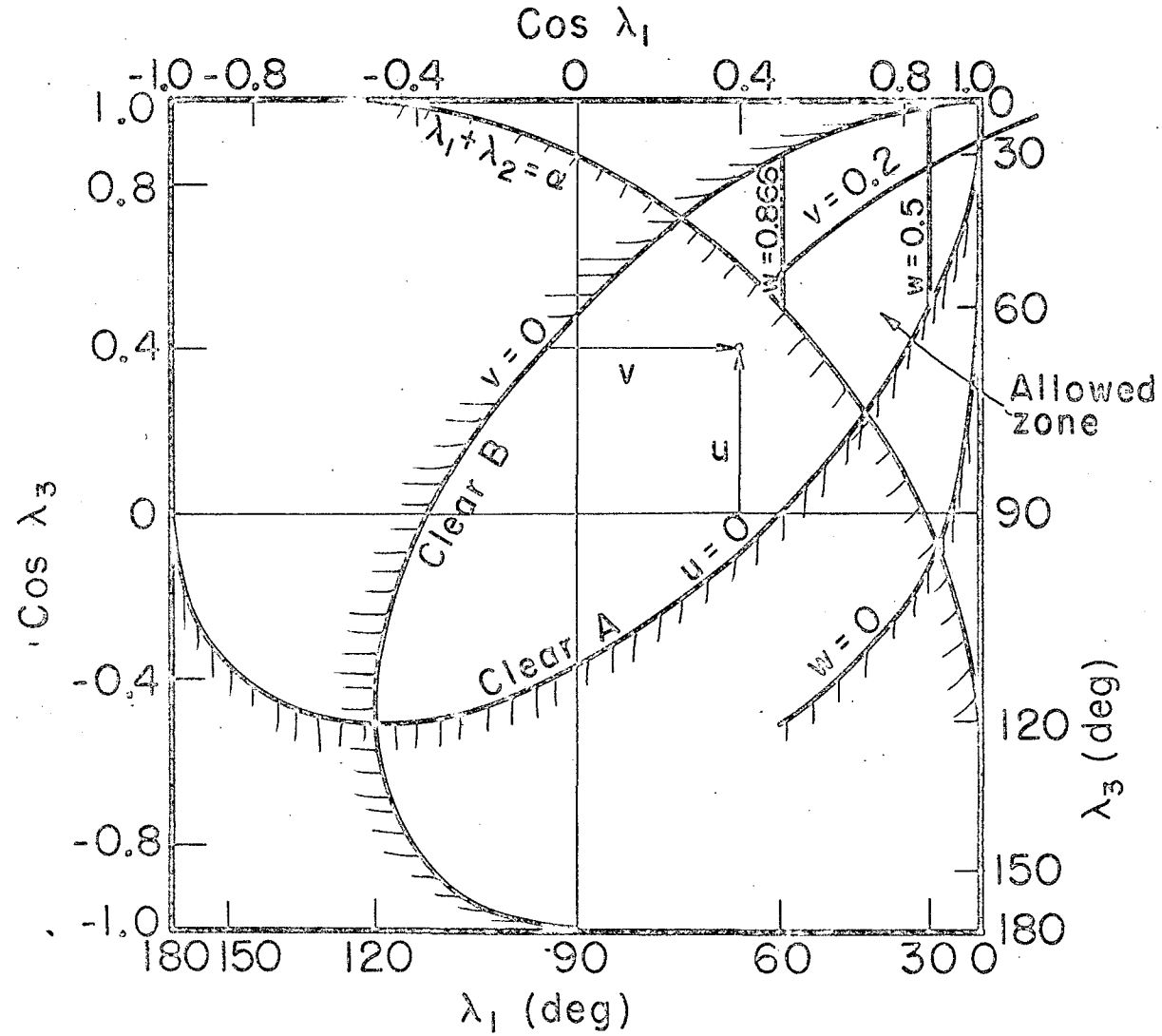

MU-26395
UCRL-10067
Fig. 3a

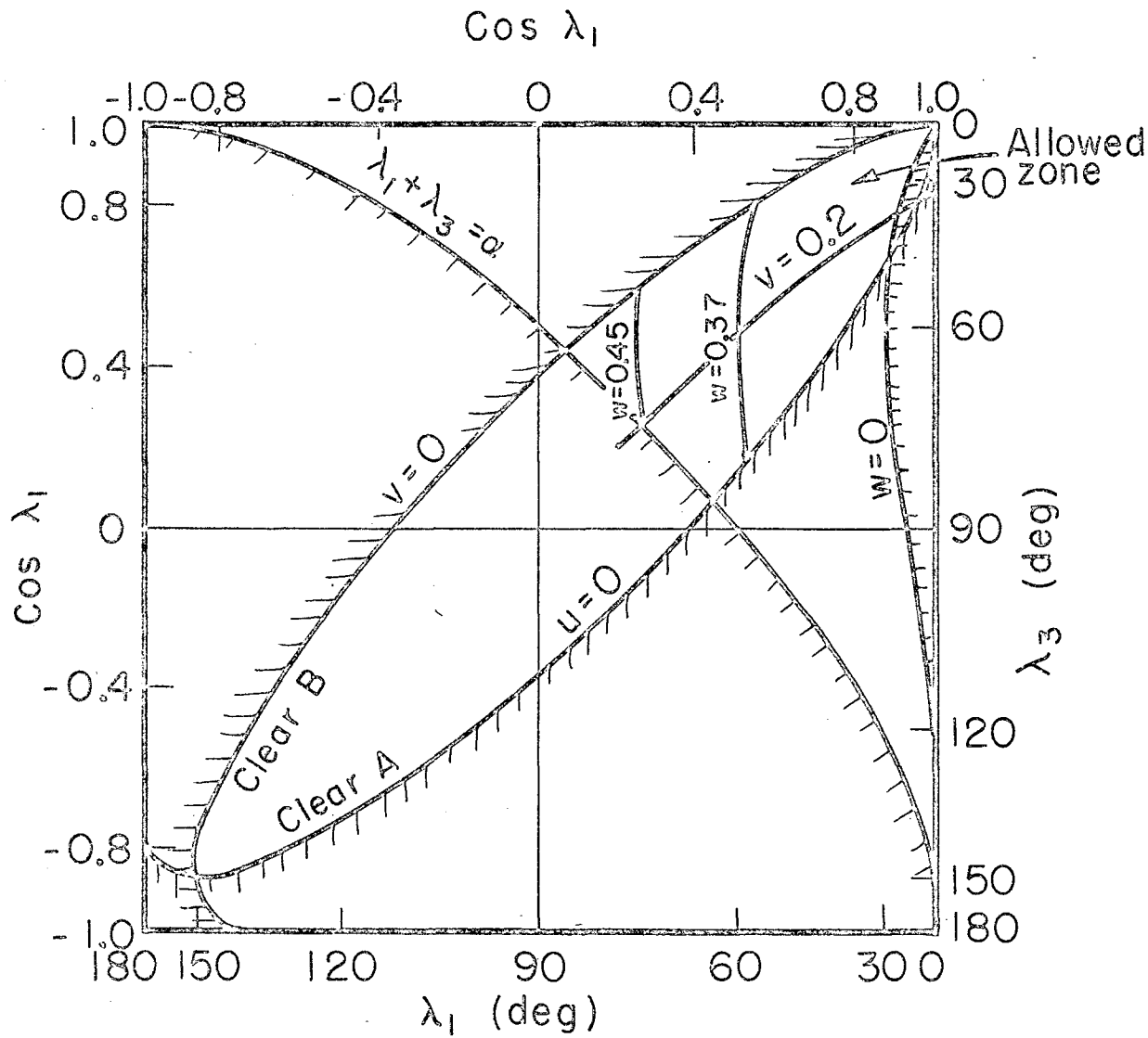

MU-26396
UCRL-10067
Fig. 3.6

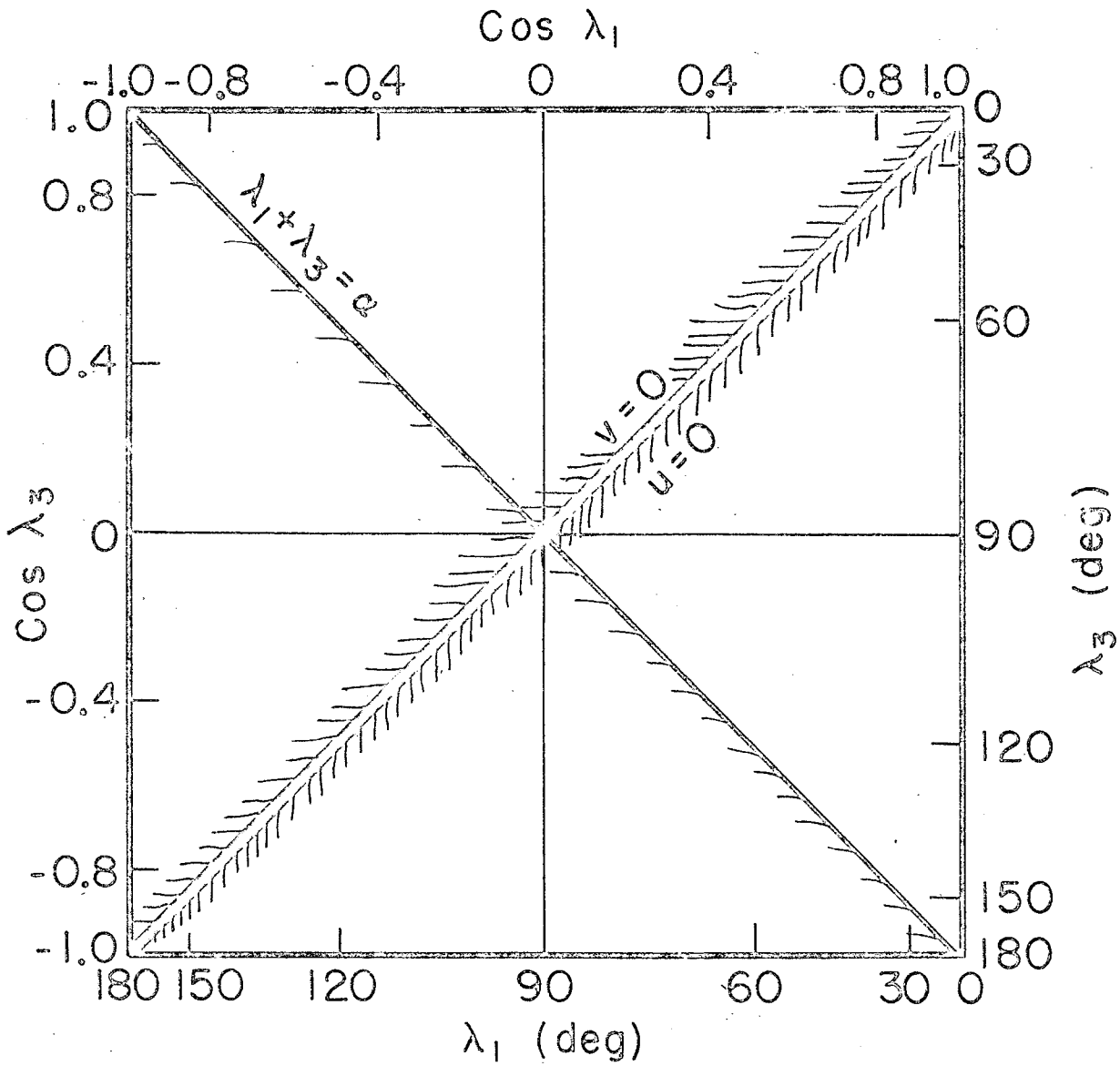

MU-26390
UCRL-10067
Fig. 3c

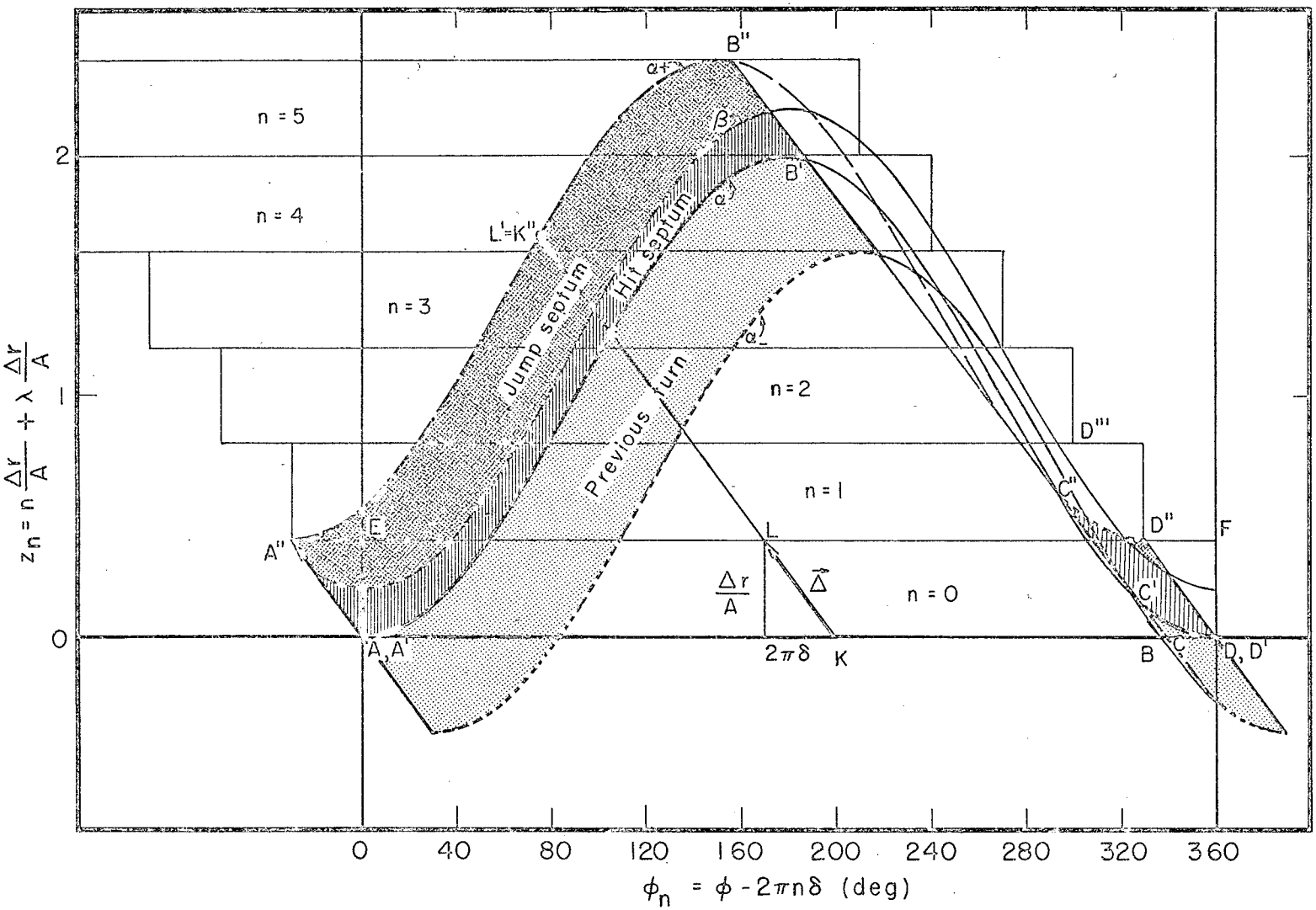

MU-26397

UCRL-10067

Fig. 4

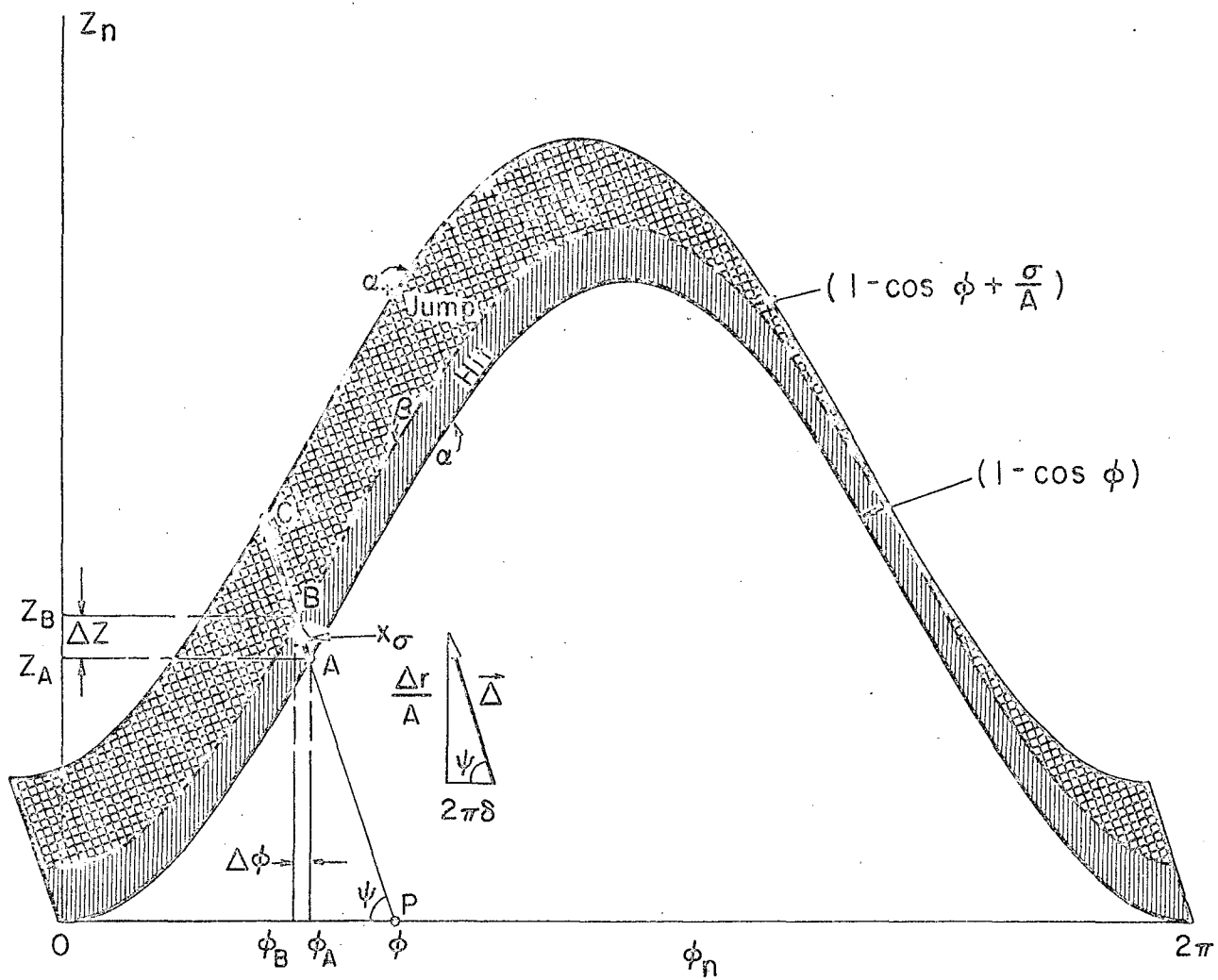

MU-26407
UCRL-10067
Fig. 5

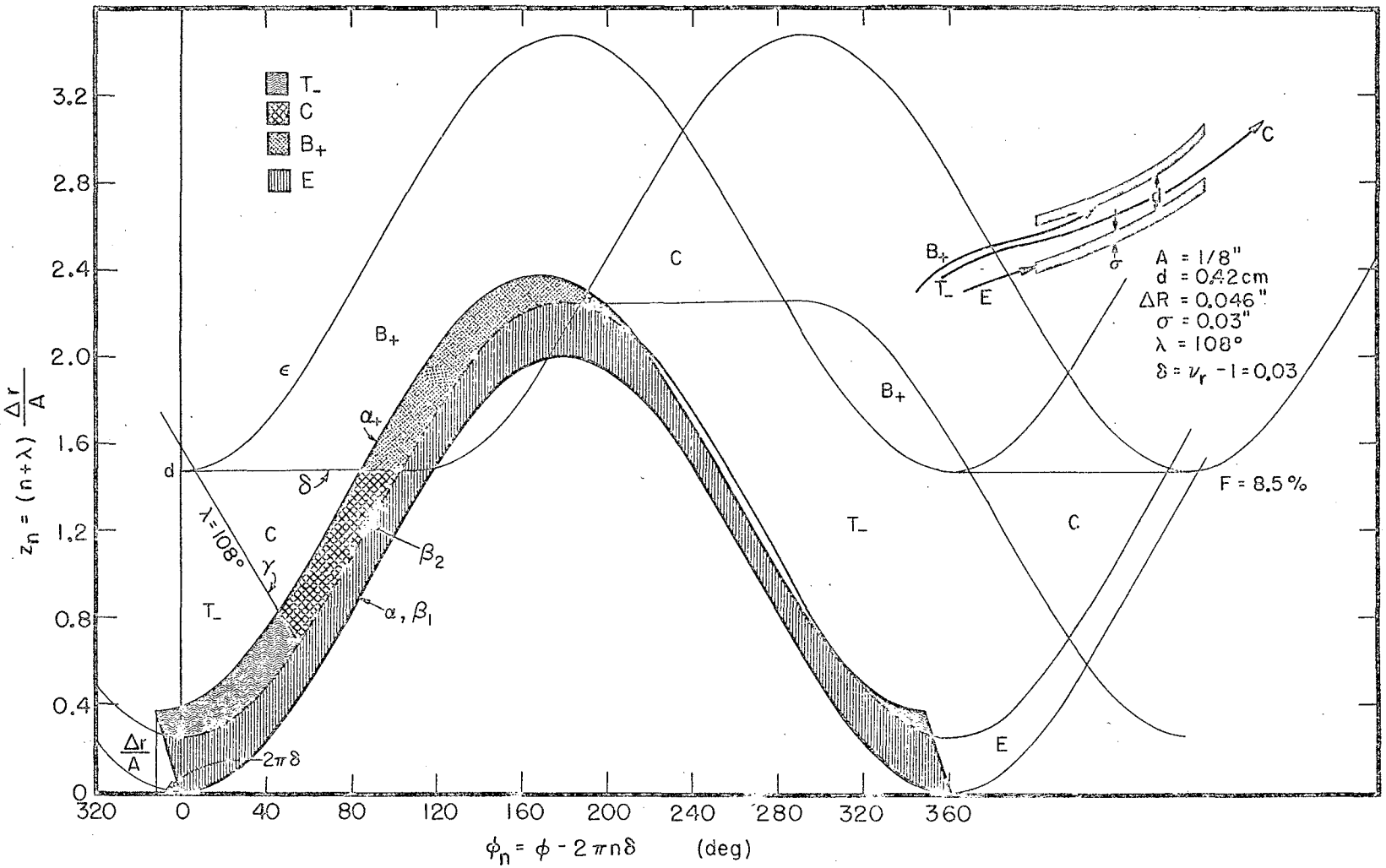

MU-26391

UCRL-10067

Fig. 6a

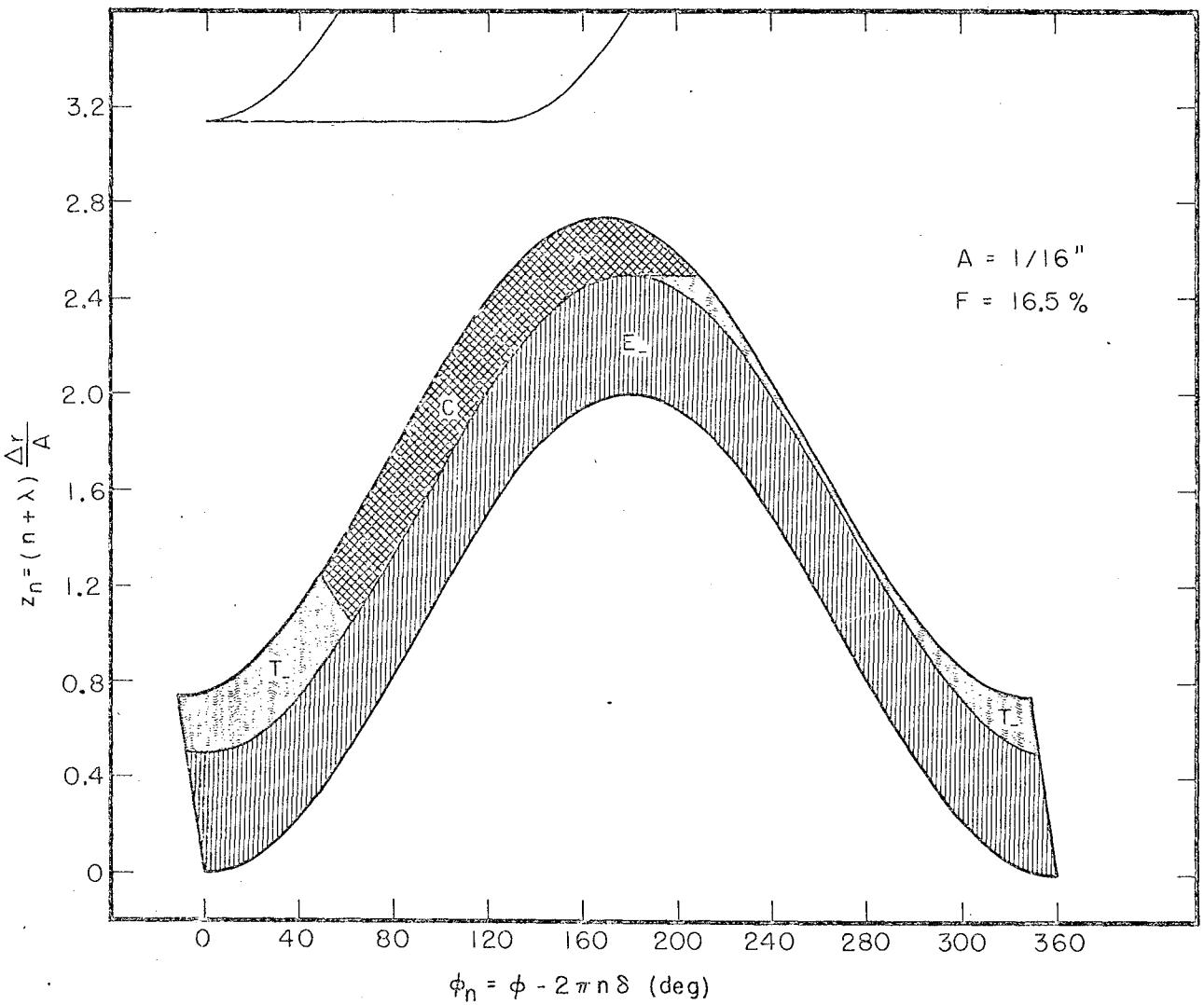

MU-26393

UCRL-10067
Fig. 6b

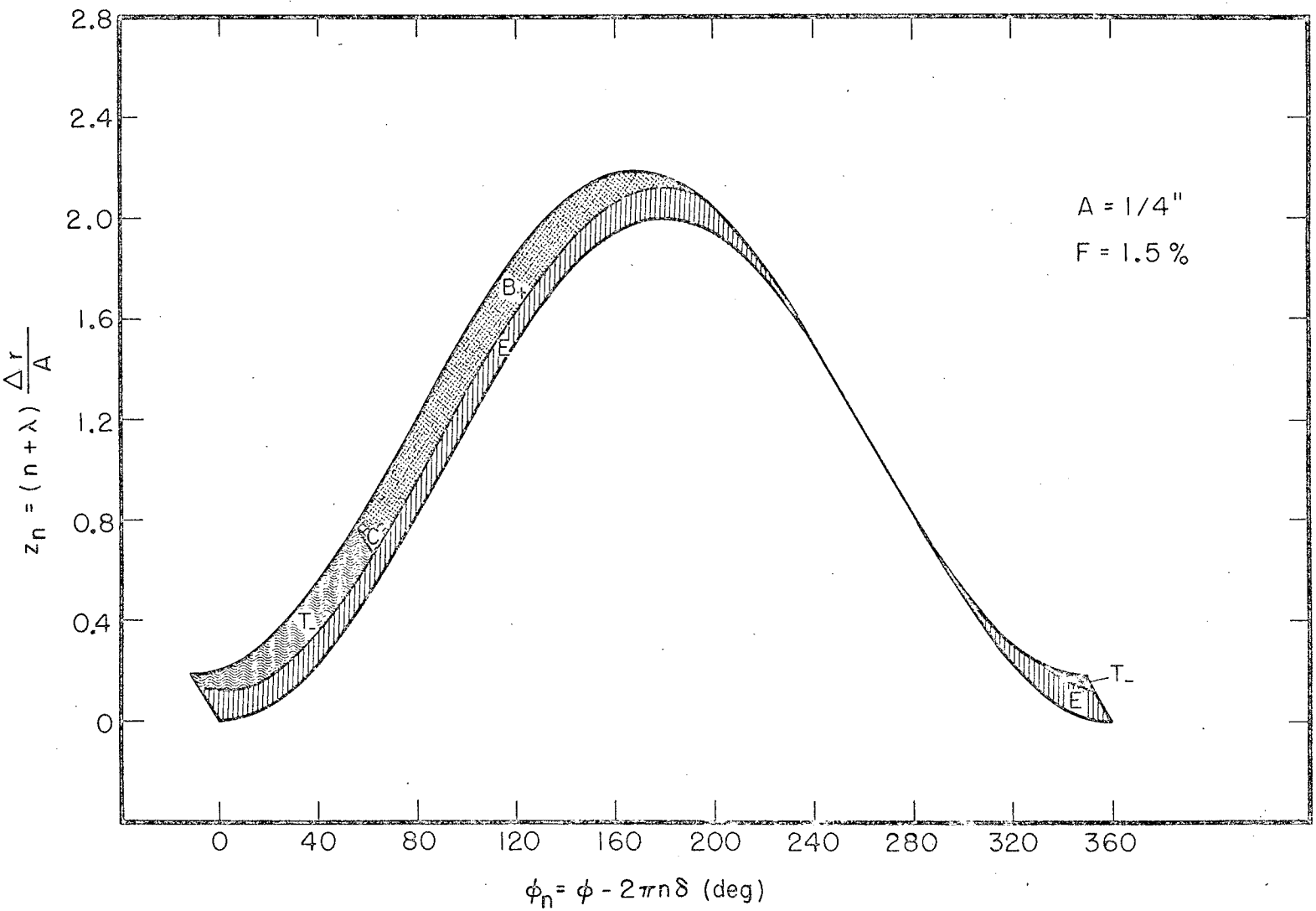

MU-26392
UCRL-10067
Fig. 6c

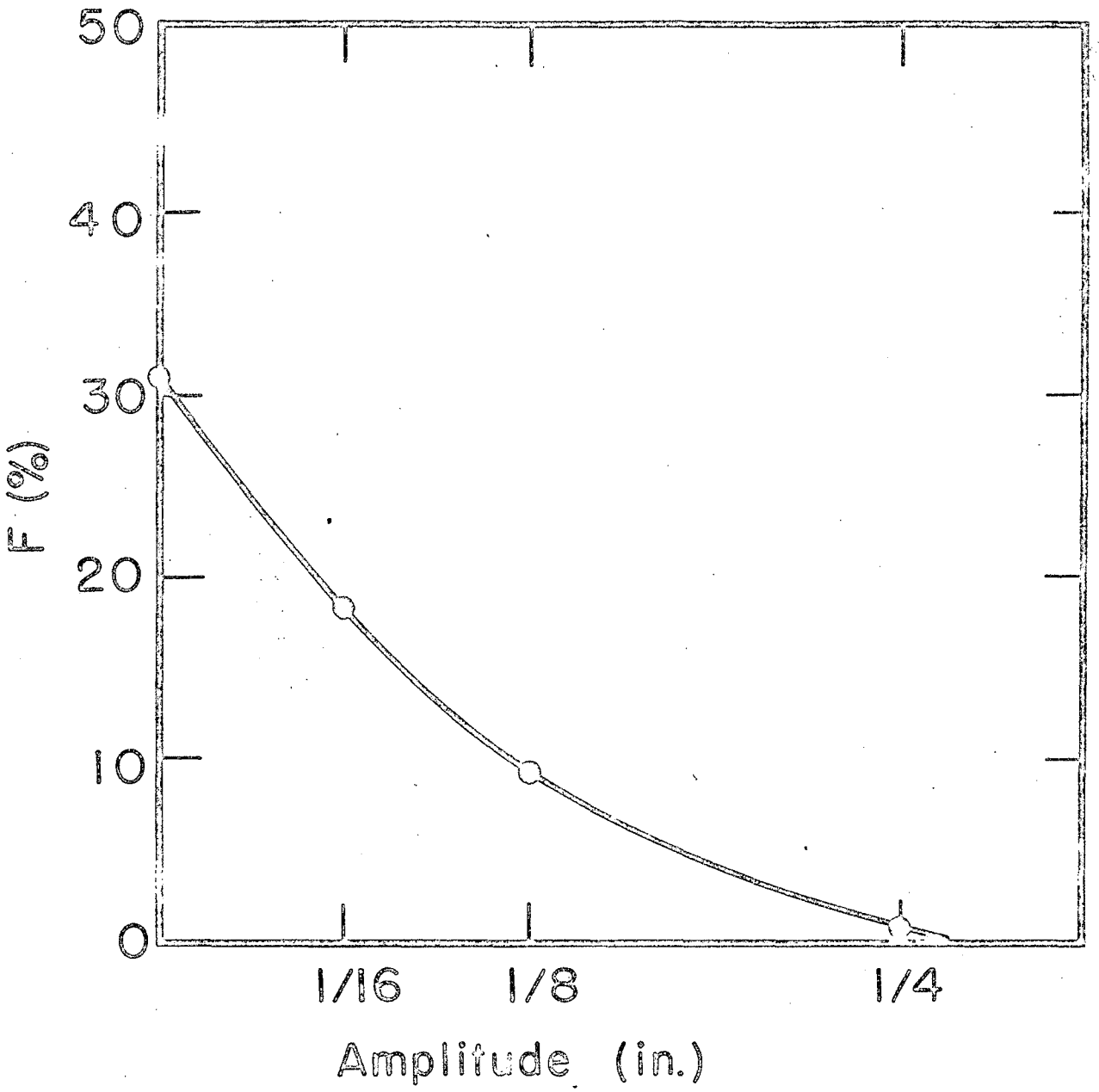

MU-26366
UCRL-10067
Fig. 6d

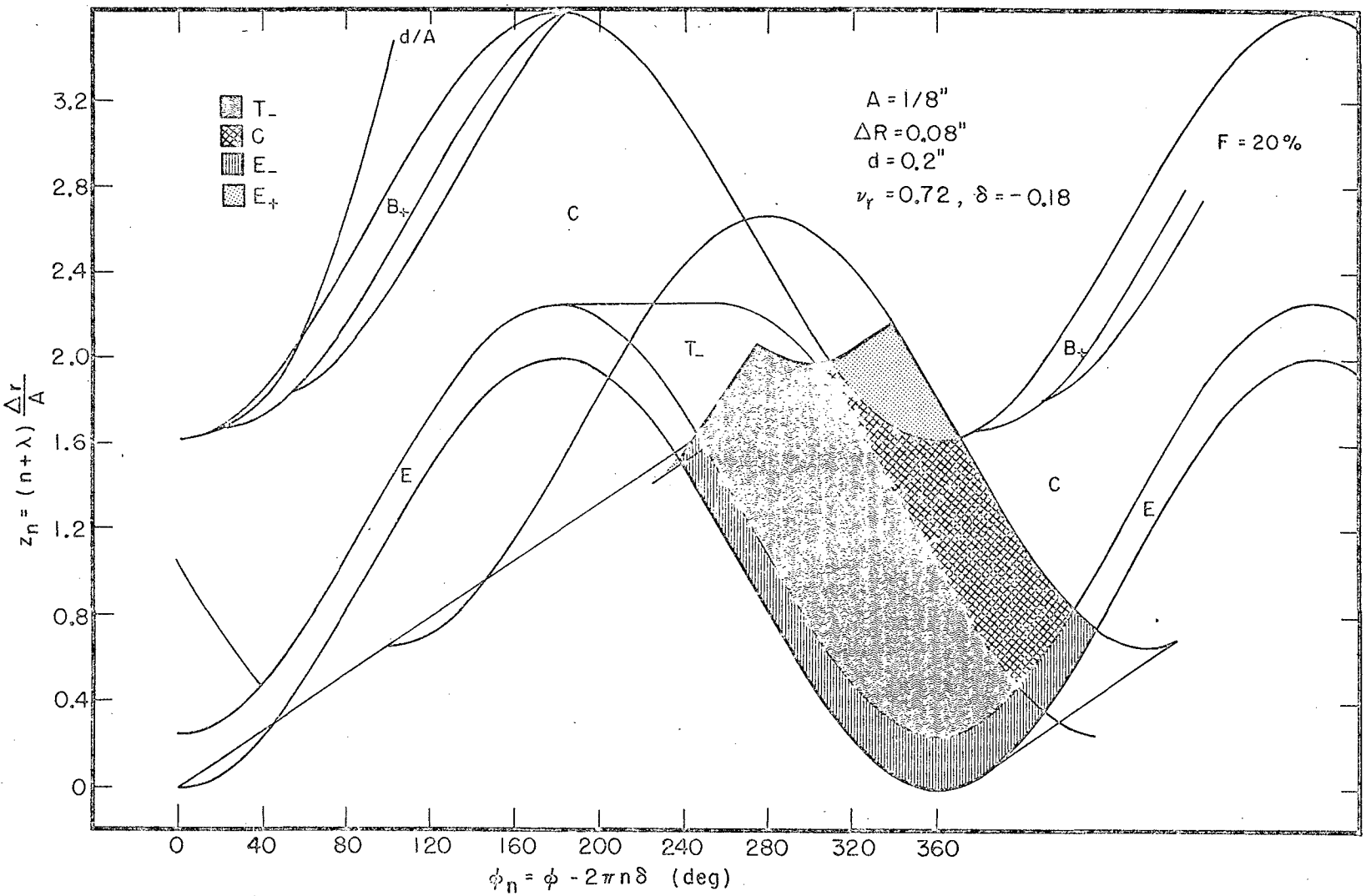

MU-26394
UCRL-10067
Fig. 7

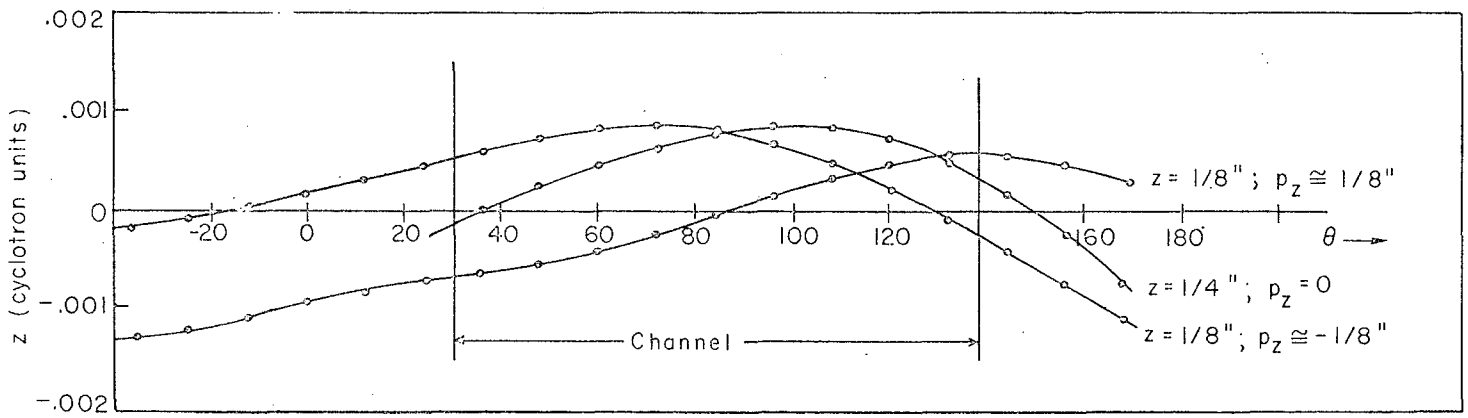

MU-26389

UCRL-10067

Fig. 8

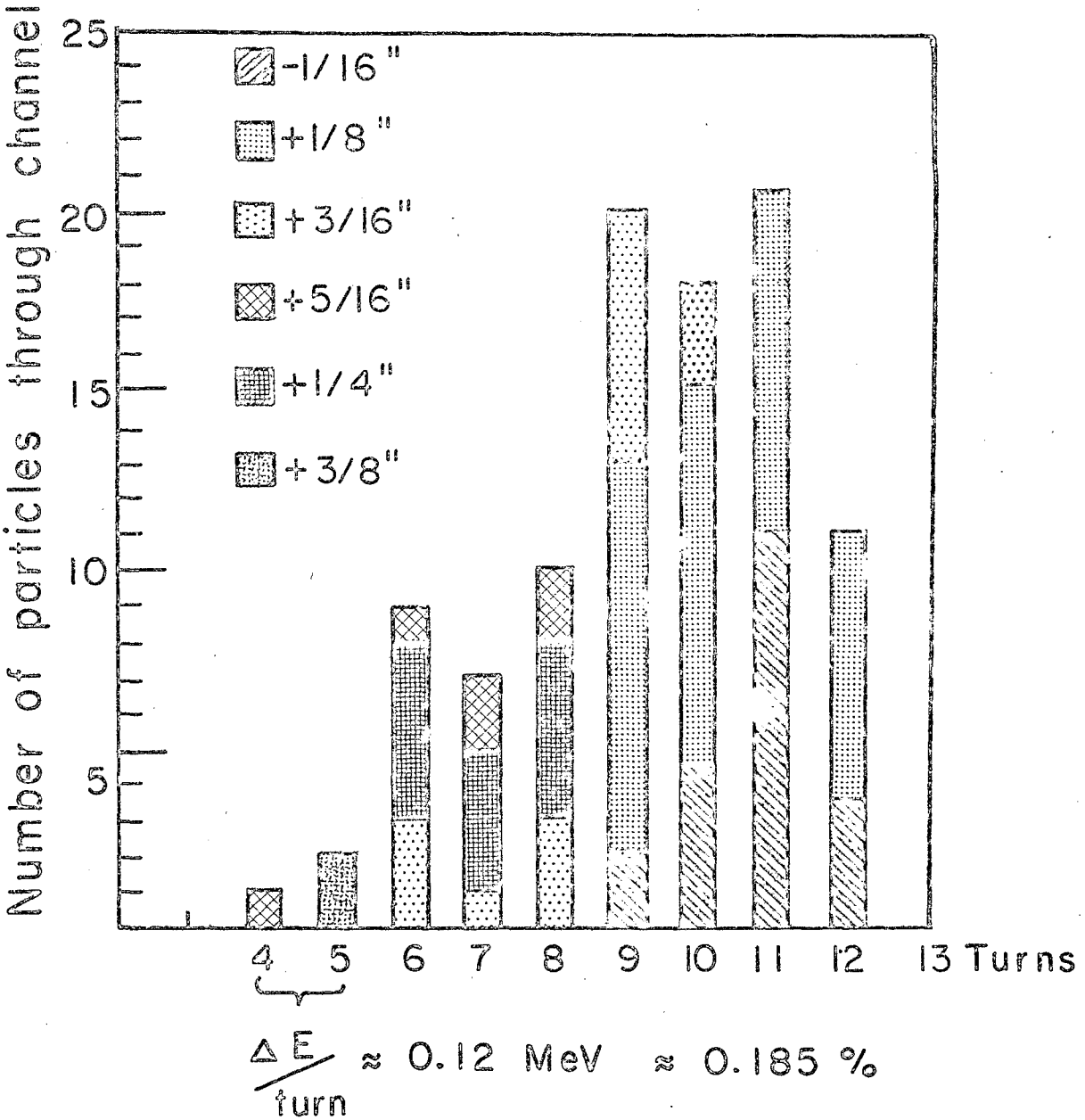

MU-26365
UCRL-10067
Fig. 9

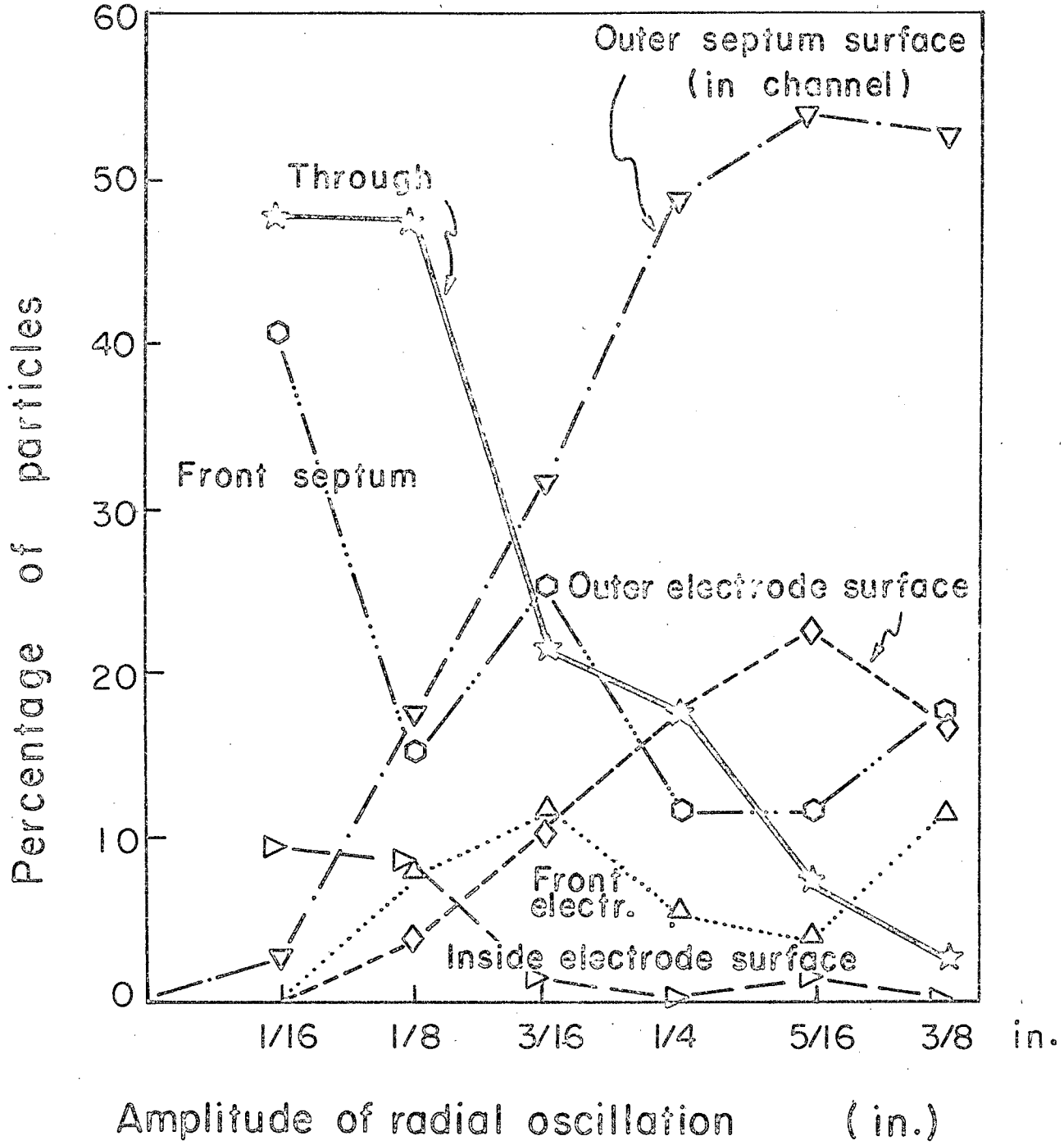

MU-26368
UCRL-10067
Fig. 10

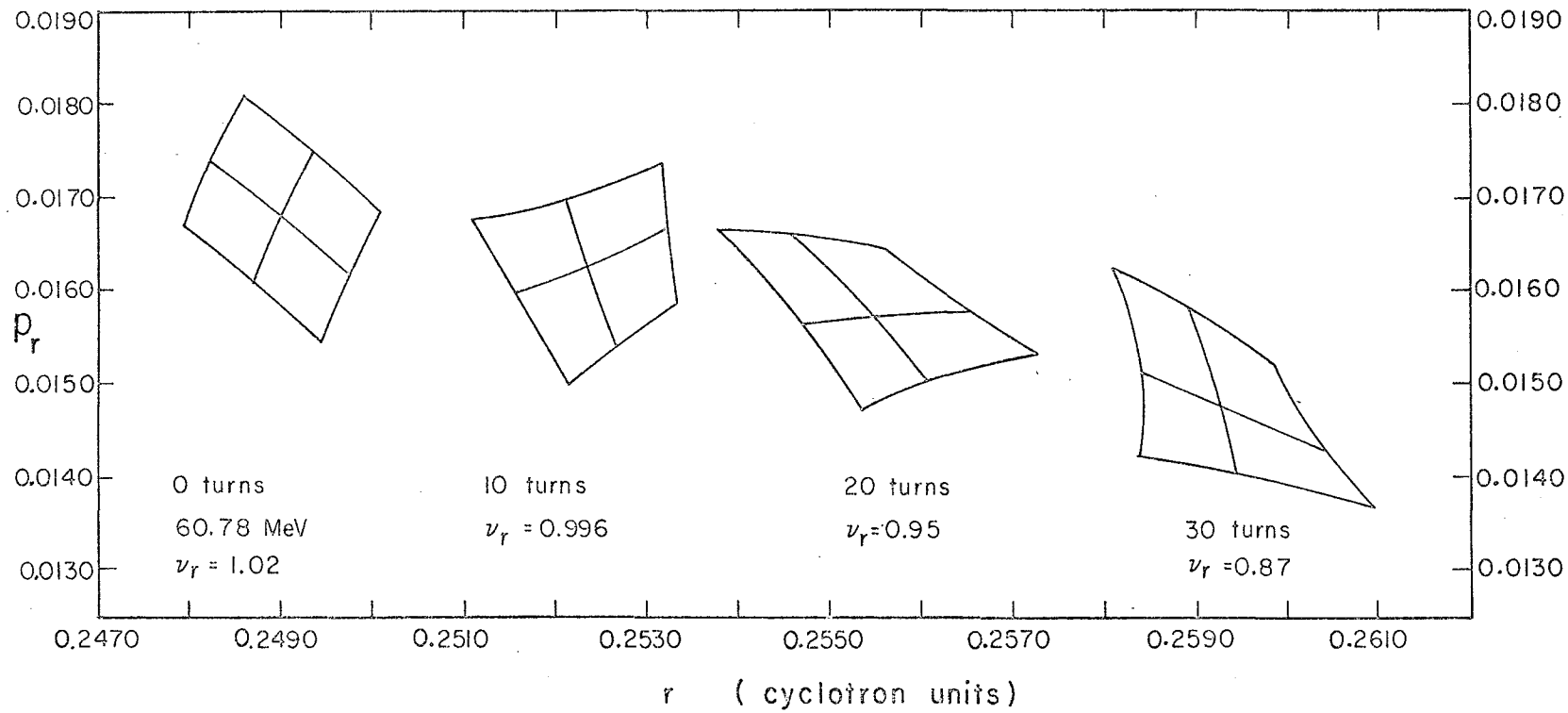

MU-26388

UCRL-10067
Fig. 11a

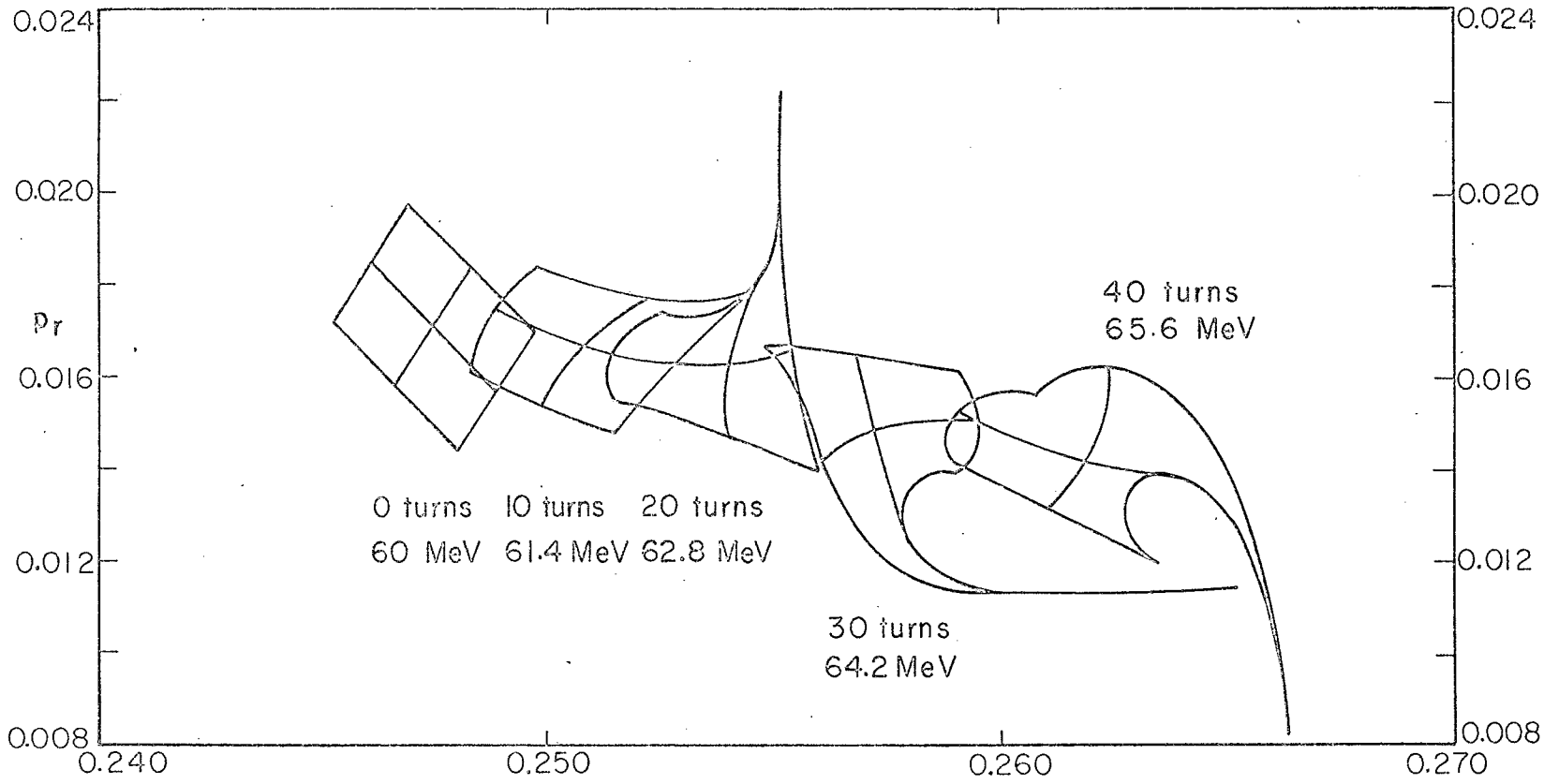

MU-26635
UCRL-10067
Fig. 11b